IOWA STATE HIGHWAY 92 OVER DRAINAGE DITCH #25

Performance Evaluation
Galvanized Reinforcing Bars

Louisa County, Iowa

Final Report
June 15, 2015
WJE No. 2012.5759

Prepared for:
Mr. Michael Todsen, P.E.
Iowa Department of Transportation
Office of Bridges and Structures
800 Lincoln Way
Ames, Iowa 50010

Prepared by:
Wiss, Janney, Elstner Associates, Inc.
330 Pfingsten Road
Northbrook, Illinois 60062
847.272.7400 tel | 847.291.9599 fax

IOWA STATE HIGHWAY 92 OVER DRAINAGE DITCH #25

Performance Evaluation
Galvanized Reinforcing Bars

Louisa County, Iowa

Jonah C. Kurth
Associate III

John S. Lawler
Associate Principal

Paul D. Krauss
Principal

James P. Donnelly
Project Manager

Final Report
June 15, 2015
WJE No. 2012.5759

Prepared for:
Mr. Michael Todsen, P.E.
Iowa Department of Transportation
Office of Bridges and Structures
800 Lincoln Way
Ames, Iowa 50010

Prepared by:
Wiss, Janney, Elstner Associates, Inc.
330 Pfingsten Road
Northbrook, Illinois 60062
847.272.7400 tel | 847.291.9599 fax

WJE ENGINEERS ARCHITECTS MATERIALS SCIENTISTS

TABLE OF CONTENTS

WJE ENGINEERS ARCHITECTS MATERIALS SCIENTISTS

IOWA STATE HIGHWAY 92 OVER DRAINAGE DITCH #25

Performance Evaluation
Galvanized Reinforcing Bars

Louisa County, Iowa

1. INTRODUCTION

Several strategies are available to the Iowa Department of Transportation (IaDOT) for limiting deterioration due to chloride-induced corrosion of embedded reinforcing bars in concrete bridge decks. While the method most commonly used throughout the Midwestern United States is to construct concrete bridge decks with fusion-bonded epoxy-coated reinforcing bars, galvanized reinforcing bars are an available alternative. Previous studies of the in situ performance of galvanized reinforcing bars in service in bridge decks have been limited. IaDOT requested that Wiss, Janney, Elstner Associates, Inc. (WJE) perform this study to gain further understanding of the long-term performance of an Iowa bridge deck reinforced with galvanized reinforcing bars.

This study characterized the condition of a bridge deck with galvanized reinforcing bars after about 36 years of service and compared that performance to the expected performance of epoxy-coated or uncoated reinforcing bars in similar bridge construction. For this study, IaDOT selected the Iowa State Highway 92 bridge across Drainage Ditch #25 in Louisa County, Iowa (Structure No. 5854.5S092), which was constructed using galvanized reinforcing bars as the main deck reinforcing. The scope of work for this study included: field assessment, testing, and sampling; laboratory testing and analysis; analysis of findings; service life modeling; and preparation of this report. In addition, supplemental observations of the condition of the galvanized reinforcing bars were made during a subsequent project to repair the bride deck.

1.1. Description of Bridge

The bridge selected for this study was constructed circa 1976 and carries eastbound and westbound traffic on Iowa State Highway 92 over Drainage Ditch #25 in Louisa County, Iowa. The location of this bridge is shown in Figure 1.1, and Figure 1.2 shows an overall elevation of this bridge. Drawings and information provided by IaDOT include: as-built drawings for the bridge, dated June 6, 1977; bridge condition survey notes, dated March 7, 2006; and proposed repair plans for the bridge, dated August 7, 2012.

The as-built drawings show the bridge as a three-span continuous slab, with a center span length of 28 feet, an overall length of 73 feet, and an overall width of 47 feet. The drawings indicate that the bridge was constructed in two stages, with a longitudinal construction joint 4 feet 8 inches to the north of the centerline of the present roadway. The northern portion of the bridge was built first, and anchor holes for a temporary traffic barrier installed onto this portion of the bridge deck during construction of the southern portion are present approximately 5 feet north of the construction joint. The bridge deck slab is 12-7/8 inches thick, and is supported directly on the abutments and piers. The deck is reinforced in the longitudinal direction with a combination of No. 7, No. 9 and No. 10 bars on top and No. 9 bars on bottom. These longitudinal bars are the main reinforcing and are located nearer to the surface than the transverse bars, which are No. 4 and No. 6 bars on the top and bottom, respectively. All bars in the deck

slab were designated as galvanized bars. Clear concrete cover was designated as 2 inches to the top bars and 1-1/2 inches to the bottom bars.

The concrete for the deck slab was designated as Class "D" structural concrete, per the Standard Specifications of the Iowa State Highway Commission, Series 1972. The drawings show that the design compressive strength for the concrete was 3,500 psi.

The deck top surface has been locally patched once, reportedly in September or October of 2009, prior to this study. IaDOT rehabilitated the bridge deck again in 2013 and 2014 after the main field work for this study was completed. The 2013-14 rehabilitation consisted of local Class A deck repairs followed by installation of a concrete overlay. In addition, both approach slabs were replaced, and the existing barrier rail was to be sealed.

1.2. Galvanized Reinforcing in Concrete

Zinc galvanizing provides protection to the underlying carbon steel of the reinforcing by providing an initial passive coating of zinc material that will act as an anode and corrode preferentially to the steel (i.e., zinc is anodic or more electrochemically active compared to steel). Galvanizing provides extended service life for the concrete primarily since the corrosion products of the zinc layer are less expansive than the corrosion products of iron, which extends the time before cracking and spalling of the concrete occurs.

Reinforcing bars for concrete structures are typically galvanized through a hot-dip process that produces a multi-layer covering of zinc and zinc-iron alloys. When exposed to freshly placed concrete, the outer layer of zinc reacts to form a passive layer of calcium hydroxyzincate. This layer provides resistance to both chloride- and carbonation-induced corrosion. This layer is stable as long as the pH is less than about 13.3 and greater than about 6, as typically occurs in concrete. The characteristics of this layer are strongly influenced by the pH within this range, and as a result, the protection provided by galvanizing is dependent on the composition of the concrete, especially by the type and alkali content of the cement (Bertolini, et al. 2004). This passive layer protects the underlying zinc and may also slow the chemical reactions that occur at the cathode sites where oxygen reacts to balance the corrosion reaction.

As with other types of reinforcing and after the zinc layer passivates within the fresh concrete, for corrosion to initiate on galvanized steel embedded in sound concrete, chloride ions must accumulate to a sufficient concentration, known as the chloride threshold, to break down the protective film. The onset of corrosion is governed by the time required for chloride to penetrate through the concrete cover over the steel and build up at the bar depth to the chloride threshold value. The chloride threshold for initiation of corrosion of uncoated black mild steel is considered to be approximately 0.2 percent by weight of cement [typically about 0.035 percent acid-soluble chloride ion by weight of concrete (or 1.0 to 1.2 lbs of chloride per cubic yard)] in typical non-carbonated concrete. Galvanized steel is generally believed to have a chloride threshold two to three times higher than uncoated steel, but some proponents of galvanized reinforcing bar suggest this multiplier may be as high as 10 (Bertolini, et al. 2004) (Broomfield 2007) (Yeomans 2004).

The concept of chloride threshold may oversimplify the protection provided to reinforcing bars by galvanization, since that concept allows for two corrosion states: non-corroding and corroding. For galvanizing bars, there is likely a prolonged intermediate stage before the widespread corrosion of the steel occurs, during which the zinc is consumed. During this intermediate phase, the zinc surface layer corrodes, forming a white corrosion by-product. This by-product is less expansive than the rust formed

by mild steel corrosion, so the corrosion of the reinforcing steel is the corrosion state of primary interest when determining concrete damage. The transition from zinc to steel corrosion is only partially captured in the chloride threshold concept.

2. TESTING METHODS

The program for characterizing the performance of galvanized bars in this bridge consisted of two main parts: field investigation and laboratory studies. The field investigation consisted of a visual survey, crack mapping, delamination survey, half-cell potential testing, corrosion rate testing, continuity testing, depth of cover measurements, and removal of core samples. In the laboratory, the following tests were performed on the core samples obtained: visual examination of the extracted bar samples, petrographic studies, chloride analysis, and determination of concrete chloride surface concentration and chloride diffusion coefficient. After the field and laboratory data had been collected, the data was analyzed and a projection of service life was developed.

2.1. Field Investigation

2.1.1. Visual and Delamination Surveys

A detailed visual examination of the selected deck area was conducted on the top surface of both lanes and shoulders of the bridge deck. In conjunction with the visual survey, a delamination survey was conducted using chain dragging and hammer sounding methods. The location and estimated area or length of observed distress, including delaminations, spalls, cracks, and patches, were documented. Typical crack widths were measured, and the crack density (lin ft/sq ft) was calculated for the bridge deck by dividing the total length of the cracks identified by the total surface area of the deck that was surveyed.

2.1.2. Cover Measurement

Ground-penetrating radar (GPR) was used to locate and determine the concrete cover over the reinforcing bars (see Figure 2.1). Scans were taken transverse to the bridge span at 5-foot intervals along the length of the bridge to assess cover over the top longitudinal reinforcing bars. Indicated depths of the top reinforcing bars on the GPR scans were calibrated for each bridge to actual depth measurements of the top reinforcing bars taken at core locations.

2.1.3. Core Sampling

Ten 4-inch diameter core samples were drilled from the top surface of the deck, as shown in Figure 2.2. Core locations were distributed across the deck surface in order to represent typical conditions. All core samples were located to intersect one or more reinforcing bars. Five of the cores were taken from areas of the deck that contained cracks and delaminations. The locations of the cores for this bridge are shown in the deck plan views contained in Appendix A. Each core hole was patched with a rapid-setting repair material.

2.1.4. Half-Cell Potential Survey

A copper-copper sulfate half-cell potential (HCP) survey was conducted to obtain an indication of corrosion risk for the reinforcing steel. HCP testing was performed in general accordance with ASTM C876, *Standard Test Method for Half-Cell Potentials of Uncoated Reinforcing Steel in Concrete* over the full survey area of each bridge using two different pieces of equipment: a single rolling wheel, as shown in Figure 2.3 and a nine-cell rolling test frame (see Figure 2.4). The single rolling wheel equipment (Proceq Canin+) is capable of close-interval (set at 3 inches for this bridge) measurements in the direction of the wheel, but requires multiple passes to cover an area. The rolling test frame measures an area 16 feet wide, but has single-point references cells that are spaced 2 feet apart. For both pieces of equipment, half-cell measurements were collected at 2.5-foot intervals along the length of the bridge using data loggers with 10 M-ohm internal impedance. Connections to the reinforcing steel were made by drilling down

through the concrete to expose individual reinforcing bars at multiple locations. Continuity at connections was verified to be less than 1 ohm between connections used for measurement.

2.2. Laboratory Studies

All of the cores and the segments of reinforcing bars removed from the deck were transported to WJE's laboratory, photographed, and assessed. The reinforcing steel segments were extracted from the cores, visually inspected, and examined to determine its state of corrosion. Selected cores were then cut or sectioned for further analyses.

2.2.1. Petrographic Examination and Carbonation Testing

One core sample was selected for petrographic analysis to characterize the overall quality and nature of the concrete, as outlined in ASTM C856-04, *Standard Practice for Petrographic Examination of Hardened Concrete*. The petrographic analysis included microscopic evaluation to assess the characteristics of the air void system, the cement paste, the soundness of the aggregate, and the water-cement ratio. Additionally, the upper regions of six cores were tested for depth of carbonation using a phenolphthalein pH indicator.

2.2.2. Chloride Content Analysis

To evaluate the existing distribution of chloride ions within the deck concrete and to permit estimates of chloride concentrations in the future, the chloride concentration profiles with depth were determined for six cores. Multiple slices were cut from these cores and ground for chloride analysis. By determining chloride concentrations at different depths, chloride profiles could be determined, from which surface concentrations and diffusion coefficients could be calculated.

To remove the slices for testing, the top approximately 1/8-in. of each of the concrete cores was removed, and the cores were sectioned to obtain 1/8-in. slices approximately centered at depths of 3/16, 11/16, and 1-3/16 inches from the original wearing surface, and at 1/16 inch above the bar depth (generally 2 to 3 inches from the deck top surface). For those cores for which a profile was not determined, a single approximately 1/8-inch thick slice was cut from the core directly above the top reinforcing bar. One additional slice was cut from an uncracked core at a depth of 6 inches to determine the background, as-built chloride concentration. The slices were pulverized for acid-soluble chloride content analysis essentially according to ASTM C1152-04, *Standard Test Method for Acid-Soluble Chloride in Mortar and Concrete*.

Acid-soluble chloride represents nearly all chloride contained in the concrete sample, including any chloride chemically bound within the paste or aggregate. Negligible acid-soluble chloride concentrations were measured in the deepest (background) core slices taken from this bridge. Consequently, measured chloride contents were presumed to be caused solely due to the application of deicing salts to the deck top surface.

2.2.3. Examination of Extracted Bars

Galvanized reinforcing bars embedded in each core were initially extracted in the lab and visually examined to characterize appearance, color, and state of corrosion. Corrosion status was categorized as uncorroded, zinc rust (white deposits), or iron rust (red deposits). The top and bottom surfaces of each bar were further described by the percentage of surface area falling into each of the three corrosion statuses.

The corrosion product on the exterior of the bar samples was evaluated visually using a stereomicroscope, and selected samples of reinforcing bar were identified for in-depth analyses of the corrosion by-product composition and of coating thickness.

Two specimens were analyzed to determine the composition of the corrosion by-product using scanning electron microscopy with energy dispersive x-ray spectroscopy (SEM/EDS). The corrosion by-products from one of these samples was further analyzed using x-ray diffraction (XRD).

The zinc coating thickness on five bars was determined by examination of cross-sections using reflected light microscopy. The bars were cut in cross-section, embedded in a thermoset epoxy resin, and polished to produce a suitable surface. The zinc layer thickness was measured around the bar perimeter using a calibrated scale reticle in the microscope eyepiece.

3. FIELD AND LABORATORY FINDINGS

3.1. Results of Field Testing

3.1.1. Visual and Delamination Surveys

Overall photos of the deck top surface are shown in Figures 3.1 and 3.2. The deterioration noted during the visual and delamination surveys is presented on the plan drawings in Appendix A.

Patching of this deck had been performed in the fall of 2009 to address the deterioration observed in 2006. A number of new delaminations have presumably developed since those repairs were installed. Squared boundaries for repair areas associated with most of the new delaminations had been marked by IaDOT staff on the deck surface, apparently in preparation for the planned 2013 rehabilitation.

A number of partial-depth, longitudinally-oriented cracks were noted that appear to follow the top reinforcing bars. The delaminations and marked repair areas appeared to be associated with many of these cracks.

The patch repairs were generally distributed uniformly across the deck surface. One long, relatively narrow (approximately 24-inch wide) repair was present at the location where the temporary barrier rail had been installed during the original construction. It is unclear whether this repair was performed to address corrosion-related distress, but it is likely that the repair was prompted at least in part by the anchor holes for the barrier rail. These holes were partially filled with grout where they remained (see Figure 3.3).

With one exception, the patch repairs were generally sound. Many of the new delaminations were located immediately adjacent to these repairs, and likely resulted from the "halo" or "ring anode" effect, a process by which corrosion of embedded reinforcing immediately adjacent to concrete repairs is accelerated by locally large differences in the internal concrete environment at the perimeter of the patch repairs. An example of a new delamination along a crack and adjacent to an existing repair is pictured in Figure 3.4.

Three of the areas located adjacent to the construction joint marked by IaDOT for repair as part of the 2013 rehabilitation showed cracking distress (see Figure 3.5), but were not identified as delaminated during WJE's survey. The cause of this distress is uncertain, but may be related to differential movement between the north and south portions of the deck, or freezing of water trapped in the construction joint.

The underside of the deck is generally in very good condition, as can be seen in Figures 3.6 and 3.7. While some signs of efflorescence were present at the construction joint and at some other cracks, indicating moisture passing through the thickness of the deck, only a few through-deck cracks were observed. No underside spalls were identified, and the only moisture staining noted at the drain penetrations was limited to localized areas (see Figure 3.8).

The quantities of cracks, delaminations, and repairs observed on deck top surface are summarized in Table 3.1. For the purposes of the service life modeling discussed in Section 4, the history of the development of apparent corrosion-related distress in this bridge deck was also calculated and is summarized in Table 3.2. These values are shown as a percentage of the deck area, and exclude the repairs associated with the temporary barrier rail, since those repairs may not be associated with corrosion-related distress. Although the quantities shown in 2006 and 2012 were based on sounding surveys, the level of distress in 2009 was estimated based on the extents of the repairs performed at that

time. It was assumed that the rectilinear repair areas made in 2009 bounded distress areas with generally rounded perimeters. Hypothetical distress areas were drawn on plan views of the existing repairs, and the total area of these distress areas was determined to establish the extent of the 2009 distress.

3.1.2. Cover Measurement

Results of the cover survey by GPR are provided in Table 3.3. As shown there, the average cover on the north and south halves of the bridge was 2.2 and 2.3 inches, respectively. This average is slightly greater than the clear cover of 2 inches specified on the original drawings. Considering the measured variation of cover, approximately 10 percent of the bars are predicted to have cover depths less than that specified.

3.1.3. Half-Cell Potential Survey

Contour maps of the half-cell potential surveys are shown on Figures A.2 and A.3 of Appendix A for the single rolling wheel and nine-cell frame, respectively. Interpretation of the half-cell results using the corrosion thresholds in ASTM C876 is not appropriate for this deck, because of the presence of galvanized reinforcement. Typically, half-cell potentials of uncoated steel embedded in concrete become more negative as corrosion develops. However, as discussed in Section 1.2, zinc is anodic (electrochemically negative) in comparison to steel in concrete, which will also result in more negative half-cell potentials. Interpretation is further complicated since the potentials of corroding galvanized reinforcing are mixed potentials of both zinc (where the coating is intact) and exposed steel (where the zinc has corroded away or been removed).

To determine if the half-cell potentials could be used to identify the condition of the galvanizing for the embedded reinforcing, the corrosion state for each core was plotted versus the measured potential at that location (see Figure 3.9), as determined by the rolling wheel contour map. The corrosion state was considered as the percentage of corrosion product on the bar for both white corrosion product (zinc corrosion) and red corrosion product (steel corrosion). The plot shows that no clear relationship was evident between the corrosion product on the bar and the measured half-cell potential.

Visual comparison of the contour maps to the delaminated and repaired areas of the deck also did not indicate strong correlation between the half-cell potentials and damaged or repaired concrete. Overall, the half-cell potential maps did not correlate with cracked or delaminated locations. However, repaired areas were generally more positive than surrounding areas, indicating that the repair was cathodic relative to the surrounding concrete. This is indicative of the ring-anode effect, and likely resulted because the repair material would not contain chloride so the reinforcing bars should be passivated within the repair, and because the zinc coating may have been removed during repairs as part of bar preparation procedures, resulting in a bare steel interface with the concrete. In addition to the correlation with repaired areas, the construction joint, running longitudinally on the north side of the centerline, was associated with more negative potentials. This may indicate increased chlorides along the joint.

3.2. Results of Laboratory Testing

Photographs of all the core samples are given in Appendix B. A description and the observed condition of the core samples are summarized in Table 3.4.

3.2.1. Petrographic Examination and Carbonation Testing

A report containing the findings from the petrographic examination and carbonation testing is provided in Appendix C, and the results are summarized as follows. The petrographic examination identified

siliceous and calcareous gravel coarse aggregate and natural siliceous sand fine aggregate in the concrete mix. The cement paste is strong and of good quality, and no pozzolans were detected. The estimated water-cement ratio is 0.38 to 0.45, and the approximate cement content is 6 to 7 bags per cubic yard of concrete. The concrete is air-entrained and contains 6.5 to 7 percent air. The air void system is judged to be adequate for proper protection of the concrete from cyclic freeze-thaw damage. No evidence of deleterious reactions, such as alkali-silica reaction, that would impact the long term durability of the deck concrete was identified in the core examined.

The measured depths of carbonation were less than 1/4 in. on five of the six cores tested. Carbonation in the sixth core extended as far as 1-1/4 in. from the deck surface adjacent to a crack. Based on the limited depth of carbonation and the concrete cover typically exceeding 2 in., carbonation is not significant to the overall corrosion of the reinforcing or durability of the deck.

3.2.2. Chloride Content

Acid-soluble chloride content test results are provided for each core in Table 3.5. Chloride content profiles versus depth are plotted in Figure 3.10; chloride contents at the bar depth are also indicated for all 10 cores. For comparison purposes, the corrosion state of the extracted bars, as described in Section 3.2.3 below, is indicated by the symbol shown for each core. Cores at cracked or delaminated locations are also identified.

The resulting chloride profiles can be grouped into three categories: cracked, uncracked, and sheltered. Observations from these profiles are as follows:

- Chloride profiles for cracked cores are represented by Cores 5 and 9, which had partial depth vertical cracks. The cores taken at cracked or delaminated locations had the highest chloride content at the bar depth, in excess of 0.180 percent by weight of concrete. These bar samples had red rust (steel corrosion) at least on the top surface of the bar and white rust (zinc corrosion) on the top and bottom surfaces of the bar.
- Chloride profiles for uncracked cores are represented by Cores 3, 4, and 8. These cores had chloride contents less than 0.060 percent by weight of concrete at the bar depth. The bars from these cores did not have any red rust (steel corrosion), but did have some white rust (zinc corrosion) evident on the bar underside.
- The sheltered core profile is represented by Core 6. This profile had the lowest surface concentration of chloride of all the cores. This core came from the shoulder of the north half of the deck near the barrier. Documentation from the 2006 inspection indicated that this area had a build-up of 2 inches of "gravel". It is unclear whether the gravel build-up had a direct effect on the chloride exposure, or whether localized drainage patterns had resulted in lower chloride exposure than on other areas of the deck. The bar extracted from Core 6 did not have active zinc or steel corrosion.

3.2.3. Examination of Extracted Bars

All bars were extracted from the cores within one week after removal from the bridge and were visually examined. Appearance of red corrosion by-product (representing steel corrosion) and white corrosion by-product (assumed to represent zinc corrosion) was catalogued as a rough percentage of the area of the top and bottom surfaces of each bar. In addition, the severity of corrosion was also noted. These observations are provided in Table 3.6, and the details of the bar examinations are included in Appendix D.

Five bars were then further examined in detail to evaluate the corrosion by-product, the degree of pitting, and the thickness of the zinc layer. The bar samples were selected to encompass the range of chloride levels within the concrete, from 0.004 to 0.376 percent by weight of concrete. The zinc coating thickness was measured at least 12 times around the circumference of cross-sections taken from the bars.

Galvanizing Thickness and Pitting

The bars are hot-dipped galvanized, and the zinc coating appears to be typical for this type of galvanizing. The zinc coating thickness in the samples exposed to low levels of chloride, 0.084 percent by mass of chloride or less, were nominally similar and averaged between 4.1 and 6.6 mils, with individual measurements ranging from 2.2 to 9.0 mils. In this range of chloride concentrations, the zinc coating thickness of the bars did not appear to be affected by chloride, and it appears that these values are representative of the original coating thickness.

Light white (zinc) corrosion stains were noted on samples from Cores 3, 4, 7, and 8 that were in chloride concentrations less than 0.084 percent. The zinc layers were intact at every location measured around the circumference of the bar. They did contain limited white corrosion by-product on the surface, most often on the underside of the bar. This underside corrosion may be due to incomplete contact with the concrete due to the minor settlement of the concrete away from the bottom of the bars, or to the trapping of bleed water beneath the bars. It is not uncommon for concrete settlement and bleed water to alter the contact area of the bottom sides of reinforcing bars supported on chairs. It did not appear that this initial zinc corrosion was due to chloride ingress within the concrete.

Significant loss of zinc thickness and underlying steel corrosion was observed in the two samples with chloride concentration greater than 0.193 percent by mass of chloride. Samples from Cores 9 and 10, which contain heavily chloride contaminated concrete, had intact zinc layers present only intermittently on the surface, and had pitting and red rust present on the surface. Sample 10, which had the highest chloride level, had the greatest amount of pitting present along the circumference studied.

Surface Analysis

The surface composition of Sample 8, chosen to represent a bar in non-chloride-contaminated concrete, consisted primarily of zinc, with some oxygen, and elements from the concrete that remained adhered to the surface. Although minimal oxidation of the surface was apparent from SEM/EDS analysis, the vast majority of the zinc layer was uncorroded. Analysis of Sample 10, chosen to represent a corroded bar in chloride contaminated concrete, indicated the presence of chloride-induced corrosion in the pits, but little chlorine present in the intact or lightly corroding zinc layer.

For all bars, the observed state of corrosion was related to the quantity of chloride at the bar level. No bars were observed with red rust (steel corrosion) for chloride contents less than 0.084 percent by weight of concrete. Conversely, all bars had red rust (steel corrosion) for chloride contents greater than 0.193 percent by weight of concrete. The presence of white rust (zinc corrosion) was not related to the chloride content in the concrete. Eight of ten bars had white rust on the underside, regardless of the chloride content. No bars had white rust on the top surface for chloride contents less than 0.084 percent by weight of concrete; apparently intimate contact with the concrete prevented zinc corrosion products from forming. Three of five bars had white rust on the top surface for chloride contents greater than 0.193 percent by weight of concrete. No cores sampled during this investigation contained bars with chloride contents between these two values, so intermediate estimates of chloride content relative to corrosion state could not be made.

4. SERVICE LIFE MODELING

Based on the findings of the field investigation and the laboratory analysis, the primary distress-causing mechanism for the bridge deck is chloride-induced corrosion of the deck reinforcement. As a consequence, the useful life of the deck is expected to be primarily controlled by the time required for corrosion–related damage to develop. To compare the performance of the galvanized reinforcement to the expected performance of uncoated or epoxy-coated reinforcement, a service life model was developed.

Service life in a given setting must be defined based on requirements unique to that structure in terms of performance and occupancy needs. From previous discussions with IaDOT, bridge decks in the state are generally considered to have reached the end of their service life when the damage on the top surface of the deck approaches 10 percent of the total deck area. End of service can be defined as when the deck should be replaced or when rehabilitation is necessary, such as deck repairs or an overlay. However, as shown by the history of distress in Table 3.2, the actual cumulative damage on the deck is approximated at about 5 percent. Since IaDOT is considering an overlay at this time, consequently this modeling considered two potential damage thresholds, one at 5 percent (representative of current estimated cumulative damage on this bridge) and 10 percent (nominal end of service life condition). For the purpose of this model, damage was considered as the area represented by a corrosion-induced delamination or spall, as would be identified in a typical visual and sounding survey.

4.1. Description of Service Life Model

4.1.1. Initiation and Propagation of Corrosion

Corrosion-related damage to concrete can be conceptualized in two stages. During the first stage, no corrosion is occurring but conditions are developing that cause corrosion to initiate, the duration of which corresponds to the initiation time (t_i). During the second stage, corrosion continues and build-up of corrosion by-product occurs until the volume of corrosion by-product exceeds the threshold needed to crack, delaminate, or spall the concrete in order to develop surface damage (delamination or spalling), the duration of which is the propagation time (t_p). This concept is illustrated by Figure 4.1 and forms the basis for the service life model. The concept of this model is well-suited for determining expected performance related to serviceability concerns, such as cracking, delaminations and spalls.

This concept can be applied to concrete experiencing corrosion-related damage by considering the sequence that leads to delamination and spalling. For a single bar location undergoing chloride-induced corrosion, this includes the following steps, as illustrated in Figure 4.2.

- First, initially after construction, the bar is embedded in fresh concrete and is passivated against corrosion. In practice, the zinc on galvanized bars will initially corrode to a small degree in the fresh, high pH concrete, but will quickly stabilize to an essentially passive state.
- Second, the concrete surface is exposed to a chloride source (e.g. deicing salts) and chloride begins to propagate into the concrete. Concrete carbonation also proceeds from the exterior surface, but is not an issue in this instance.
- Third, after some time has passed, the chloride reaches the bar and begins to build-up. The passivation of the bar is lost when the chloride concentration exceeds the chloride threshold, and corrosion initiates at the surface of the bar closest to the face of the concrete element exposed to chlorides.
- Fourth, chlorides proceed deeper into the concrete, and corrosion propagates around the bar.

- Fifth, corrosion products on the bar have built up to a sufficient level to cause cracking, delaminations or spalls in the concrete that become detectable from the surface.

4.1.2. Probabilistic Approach

An established probabilistic modeling approach developed by Sagüés (Sagüés 2003) was adapted and used as the basis for the service life model. This approach determines the amount of deck area affected by corrosion based on statistical distributions of key parameters considered to govern corrosion initiation. This model also recognizes the fact that corrosion is a local process that develops at multiple locations at different times.

At a given location, corrosion initiation is defined as the time required for the chloride concentration to exceed the threshold at the bar depth. Time-to-corrosion initiation is considered as a probabilistic variable influenced by combinations of independent random variables. This process can be described mathematically as follows (Bastidas-Arteaga, et al. 2011):

Corrosion initiation time is governed by a joint probability distribution, which is a function dependent on the slab:

$$f(\underline{x}) = f(chloride\ exposure, transport\ rates, corrosion\ threshold\ ) \qquad \text{Eq. 4.1}$$

where $\underline{x}$ represents the vector of random variables, and $f(\underline{x})$ represents a function of their joint probability distribution. Corrosion initiates when the given deterioration mechanism reaches a particular bar depth. The initiation time at a given location is then defined by a limit state function:

$$g(\underline{x}, t) = d_{crit} - d(\underline{x}, t)\ \ where \begin{cases} g(\underline{x}, t) \le 0, & corrosion\ initiation \\ g(\underline{x}, t) > 0, & no\ corrosion \end{cases} \qquad \text{Eq. 4.2}$$

where $d(\underline{x}, t)$ is the depth of the deterioration mechanism at a given time t, and d_{crit} represents the depth of cover. Combining the two statements, the probability that the reinforcing steel at any point in the slab has started to corrode is calculated by integrating over the failure domain:

$$p_f = \int_{g(\underline{x},t)\le 0} f(\underline{x}) d\underline{x} \qquad \text{Eq. 4.3}$$

The probability of failure with respect to a single location can then be abstracted to the performance of the deck as a whole. If the deck is of sufficient size for multiple, independent locations of corrosion-related damage to develop, it can be discretized into a large number of segments with properties defined by statistical distributions either measured or assumed. The cumulative probability of the deck segments exhibiting damage through a given time then can be used to determine the percentage of the area of the deck damaged versus time.

After corrosion initiates, corrosion by-product builds up until a crack propagates to the concrete surface, and a delamination or spall is caused in the surrounding concrete. The total time to damage is then given as a combination of initiation time t_i and the propagation time t_p. Propagation time is often chosen as a fixed value or is based upon observed damage levels for a particular bridge deck.

$$t_{damage} = t_i + t_p \qquad \text{Eq. 4.4}$$

Because of the complexity of the required analysis, a Monte Carlo simulation was run to account for the interaction between the variables considered. Latin Hypercube Sampling was used to reduce the number of segments required for model convergence (Wyss and Jorgenson 1998).

4.1.3. Chloride Ion Transport

Chloride ion transport in concrete is complex and may occur through diffusion (caused by chloride ion concentration gradient), capillary absorption (wetting and drying), and permeation (driven by pressure gradients) (Stanish, Hooton, & Thomas, 1997). Chloride transport may also be slowed by chemical binding of the chlorides with aluminate phases in the cement, or by physical absorption or trapping of chloride ions in pores. Despite the potential complexity of the chloride penetration process in concrete, it is commonly assumed that diffusion plays the largest role. Therefore, describing chloride transport by using a mathematical representation of diffusion, quantified based on an "apparent" diffusion coefficient calculated from chloride concentration profiles measured in the actual structure, is judged to be a reasonable representation of this process accounting for other influences (Sohanghpurwala, 2006).

The driving force behind the diffusion process is the chloride exposure, or the amount of chloride applied to the concrete surface. This is quantified in terms of the effective surface chloride concentration, C_s. Chloride diffusion in concrete, driven by a concentration gradient, can be described by Fick's Second Law of Diffusion:

$$\frac{\partial C}{\partial t} = D_a \frac{\partial^2 C}{\partial x^2} \qquad \text{Eq. 4.5}$$

where C is the chloride concentration at a depth of x from the concrete surface at time t, and D_a is the chloride diffusion coefficient.

If the surface chloride concentration C_s and D_a are assumed to be constants, the concentration $C(x, t)$ through a uniform medium at depth of x and time t is given by the following solution:

$$C(x,t) = C_s - (C_s - C_0) \times \text{erf}\left(\frac{x}{2\sqrt{D_a t}}\right) \qquad \text{Eq. 4.6}$$

where erf() is the Gaussian error function, and C_0 is the background or original chloride concentration.

The closed-form solution above is not readily adaptable for modeling variations of exposure or material properties with time. Consequently, a finite difference solution for determining chloride concentration with depth over time was used. This solution is based on a Crank-Nicholson discretization of Equation 4.5, for which the general form is provided below (Chapra and Canale 2002).

$$D_a[V_{i+1} - 2(D_a + K)V_i] + D_a V_{i-1} = -D_a U_{i+1} + 2(D_a - K)U_i - D_a U_{i-1} \qquad \text{Eq. 4.7}$$

where
i = current slice
D_a = apparent diffusion coefficient
U = concentration at timestep j
V = concentration at timestep j+1

$K = \frac{(\Delta X)^2}{\Delta T}$, where X = depth and T = time

4.2. Model Parameters Considered

The following sections describe the processes by which statistical distributions were determined for the interacting factors that govern corrosion initiation and propagation. For this investigation, initiation of corrosion was considered to be governed largely by the following properties:

- Chloride surface concentration (chloride exposure)
- Apparent diffusion coefficients (resistance to chloride ingress)
- Chloride-induced corrosion threshold
- Concrete cover over reinforcing
- Crack density
- Propagation time

Table 4.1 lists the statistical distributions and associated parameters for chloride exposure, concrete properties, and geometric properties derived from the survey of this bridge deck and considered for the model. Table 4.2 provides the chloride-induced corrosion thresholds and propagation times used for comparison among galvanized, uncoated, and epoxy-coated bar performance. The basis for quantification of the values in these tables is discussed in the following sections.

4.2.1. Chloride Surface Concentration

Values of chloride surface concentration (C_s) are strongly influenced by the exposure conditions (i.e., severity of deicing salt application). Based on studies of bridge decks in northern states conducted by WJE, C_s can range from greater than 0.80 percent by weight of concrete in New York to 0.15 percent by weight of concrete in Virginia (Lee and Krauss 2003). Exposure conditions may be characterized as follows based on C_s (Krauss, Lawler and Steiner 2009):

- mild: up to 0.25 percent by weight of concrete
- moderate: 0.25 to 0.45 percent by weight of concrete
- severe: 0.45 percent by weight of concrete or higher

For this bridge deck, values of C_s were determined based on the chloride concentration profiles determined by laboratory analyses described in Section 3.2.2. The exposure was assumed to be bi-linear, such that the surface concentration was equal to zero in the first year and built up to a level that was constant after the fifth year. With this assumption, a non-linear least-squares error fitting algorithm was used to find C_s based on diffusion as represented by the finite difference discretization. The resulting

average calculated C_s for the bridge was 0.416 percent by weight of concrete, which would correspond to a moderate exposure of deicing salts. For comparison, a previous study of eight bridges in Iowa by WJE calculated C_s values ranging from 0.557 to 0.823 percent by weight of concrete (Wiss, Janney, Elstner Associates, Inc. 2011). Lower traffic volumes on State Highway 92 Bridge over Drainage Ditch #25 might explain the slightly lower surface chloride contents as compared with interstate highway and other major highway bridges elsewhere in Iowa.

4.2.2. Apparent Diffusion Coefficients

For the purpose of the model, apparent diffusion coefficients (D_a) were considered separately for uncracked and cracked regions, in recognition of the fact that chloride transport is likely to occur more rapidly through cracks. Areas treated as cracked concrete in these analyses are based on the occurrence of cracking measured during the field survey and on the treatment of cracking discussed below in Section 4.2.3. Apparent diffusion coefficients were determined based on a least-squares error fit of the finite difference discretization to measured chloride content data from cores taken in both uncracked and cracked areas.

Calculated apparent diffusion coefficients for typical bridge deck concrete can vary widely. According to *Guidelines for Selection of Bridge Deck Overlays, Sealers, and Treatments*, apparent diffusion coefficients for typical uncracked bridge deck concrete may range from very low (0.05 in.^{2}/yr.) to high (0.30 in.^{2}/yr.) (Krauss, Lawler and Steiner 2009). A similar range of values, 0.029 to 0.242 in.^{2}/yr., was reported in a previous study conducted by WJE in 2010 for eight bridge decks in Iowa (Wiss, Janney, Elstner Associates, Inc. 2011). The average value determined for uncracked concrete in this deck was 0.036 in.^{2}/yr., which corresponds with a very low rate of apparent chloride diffusion in uncracked concrete.

In contrast, apparent diffusion coefficients calculated in cracked regions were more than three times greater, with an average calculated value of 0.118 in.^{2}/yr. This value is somewhat less than reported in WJE's previous study in 2010 for crack locations, which averaged 0.165 in.^{2}/yr.

4.2.3. Cracking Density

Crack lengths and orientation were measured during the visual field survey. Correlation was observed between cracking and deterioration, such that approximately 75 percent of the observed delaminations or repairs were associated with cracks. A crack-affected width (i.e., the width of the area around each crack where damage is assumed to be affected by that crack) of 12 inches was determined to apply to the deck based on the width of delaminations and spalls oriented along cracks as observed during the field studies. With these assumptions, the overall cracking density of 0.10 ft / sq. ft. resulted in a crack-affected area of 10 percent for the model. Because cracks are assumed to have a higher diffusion rate than sound concrete, the crack affected area has a strong influence on deck service life.

4.2.4. Concrete Cover

Concrete cover was modeled based on the depths measured by GPR scans. The data was aggregated to represent the entire deck and compared to various statistical distributions. A lognormal distribution was determined to have the best fit for the data. Lognormal distributions are only defined for ranges greater than zero, and as such are suitable for modeling concrete cover, which in practice cannot be negative.

4.2.5. Chloride Threshold

As discussed in Section 1.2, for corrosion to initiate in reinforcing steel, chloride ions must accumulate to sufficient concentration, known as the chloride threshold, to disrupt the passivity of the steel or the galvanized zinc surface. Although multiple factors (cement content and chemistry, moisture conditions, steel chemistry, etc.) affect the influence of chloride concentration on corrosion, the chloride content at the bar level was assumed to be the primary factor responsible for corrosion initiation in the deck. As discussed previously, the corrosion initiation process for galvanized bars likely includes multiple phases whereby the zinc begins to corrode and is consumed, while the steel corrosion begins slowly and accelerates as more steel surface is exposed. For modeling purposes, it has been assumed that the transition from non-corroding to corroding conditions can be represented by a single event. It has also been assumed that chloride initiation occurs for at a single, deterministic value for all types of reinforcing considered, but this too is a simplification.

Since the laboratory investigation identified widely but somewhat separated upper and lower bounds for the corrosion threshold for galvanized bars, the galvanized bars threshold was studied with three different values, and the results of the modeling were compared with the known historical development of damage on this bridge. These values were determined based on the results of the laboratory study, using an upper bound of 0.188 percent by weight and lower bound of 0.095 percent by weight for chloride levels at bars identified with and without red rust (steel) corrosion, respectively. Additionally, a "best fit" value, based on comparing measured damage to modeled damage, of 0.120 percent by weight was chosen between these two values.

To compare and contrast the effect of bar material on expected service life, additional cases were run to project the performance of the Highway 92 Bridge if it had been constructed with uncoated and epoxy-coated bars, based on the same controlling input parameters (cover, exposure, diffusion coefficient, and crack density). The chloride threshold for uncoated bars was taken as 0.035 percent by weight. Chloride threshold for epoxy-coated bars was observed to range from 0.179 to 0.286 percent by weight of concrete in WJE's recent investigation of the performance of epoxy-coated bars in Iowa bridge decks (Wiss, Janney, Elstner Associates, Inc. 2011). The lower threshold represents the lower bound on chloride concentration for corroding bars taken from deck where the top bar was coated and the bottom bar was uncoated, and the upper threshold represents the threshold where both the top and bottom mat of bars were coated. For comparison with the galvanized reinforcing, the lower bound of chloride threshold for epoxy-coated reinforcing was conservatively selected and rounded to 0.180 percent by weight of concrete.

4.2.6. Propagation Time

Previous research by others identified that the propagation time (t_p) is dependent on cover depth, properties of the concrete and steel/concrete interface, type of corrosion by-products, size of reinforcing, and corrosion rate (Liu and Weyers 1998), (Vu, Stewart and Mullard 2005). For simplification of the model, a single deterministic value was assumed for propagation time for each case considered.

Propagation times for the galvanized bars were calibrated based on field-surveyed levels of damage, as estimated for 2006, 2009, and the current study. Calibration of this parameter for the galvanized bars was performed by allowing propagation time to vary for a given assumed corrosion threshold and choosing a value that resulted in a best fit to the measured damage.

The propagation time chosen for uncoated bars was 5 years, and is a typical value assumed for this type of modeling. The propagation times for epoxy-coated bars were selected to be either 12 or 23 years, which covers the range of values determined during previous work on Iowa bridge decks (Wiss, Janney, Elstner Associates, Inc. 2011).

With this approach to calibrating propagation time, the propagation times developed for the galvanized bars ranged from 5 to 18 years depending on the associated chloride threshold; the longer t_p is associated with a lower threshold, while the shorter t_p is associated with a higher threshold. These values for galvanized bars fall within the range between uncoated bars (5) years and epoxy-coated bars (12 to 23 years).

4.3. Modeling Results

Multiple cases were run for the service life model to evaluate the expected performance of uncoated, galvanized, and epoxy-coated bars. These cases varied in the parameters for corrosion threshold and propagation time, as described above and as shown in Table 4.2. The results of the service life model, in terms of damage (area of deck exhibiting corrosion-related delamination or spalling) versus time is plotted in Figure 4.3. The figure shows results with the parameters considered for uncoated bars (black), galvanized bars (blue), and epoxy-coated bars (green). The range between the parameter estimates for similar materials is shaded.

Measured damage on the deck, as determined in 2006, 2009, and 2012, is also shown on the figure. The range bars on the measured damage indicate the approximate level of uncertainty with the data, which WJE estimated as follows:

- Based on the nature of the data collected during IaDOT's 2006 survey, which did not appear to be focused on quantities, the damage in 2006 was considered to possibly be underestimated by as much as 50 percent.
- Damage in 2009 was calculated by estimating the size of delamination expected to be present at the locations of the observed patches; however, similarly sized patches could have been associated with smaller damage areas, and the estimated quantity was considered to possibly overestimate actual damage by up to 25 percent.
- The service life model projects the evolution of damage in the absence of repairs. However, the presence of repairs may have served to slow the progression of damage. Since the actual damage may be less than the area of damage expected from the model and WJE's method for estimating damage in the repair areas may actually overestimate damage, the 2012 survey by WJE was considered to have an error of either over- or under-estimation of up to 20 percent.

The predicted damage evolution for galvanized bars in Figure 4.3 shows generally good agreement with the damage history for all three modeled cases, considering the uncertainty outlined above, when the assumed chloride thresholds (representing the lower bound, "best estimate" and upper bound based on the laboratory investigation) are paired with the appropriate propagation time (i.e., when the lower threshold is paired with higher propagation time and vice versa). Because the selected chloride threshold effectively controls the slope of the damage curve, chloride thresholds outside the upper and lower bounds found by the laboratory studies would not fit the measured progression of damage.

As previously discussed, both five percent and ten percent areas of damage were considered as the end of service life for the structure. The expected age to reach damaged areas of five percent and ten percent was

determined for each set of materials and conditions considered. The performance of galvanized and epoxy-coated reinforcement was compared to uncoated reinforcement, as shown in Table 4.2. Considering the five percent damage threshold (considered most applicable to this structure as the time to receive an overlay) and the assumed ranges of chloride thresholds and propagation times for each case, the service model results indicate the following:

- Uncoated reinforcement had an expected service life of 14 years.
- Galvanized reinforcement is projected to have a service life ranging from 35 to 41 years. As a result, galvanized reinforcement provides a much greater service life than uncoated reinforcement, with a service life extension of 21 to 27 years.
- Epoxy-coated reinforcement is projected to have a service life ranging from 46 to 58 years. Therefore, epoxy-coated reinforcement offers an extension of 32 to 44 years of service life over uncoated reinforcement, and 11 to 17 years as compared to galvanized reinforcement.

These findings are intended to represent the relative performance of bridge decks with the three types of reinforcing considered. The above values are applicable to the exposure conditions, concrete quality, and cover represented by this bridge deck. Results may be different with faster transport rates of chlorides to the bar depth on other structures.

5. DISCUSSION

Evaluation of the Iowa State Highway 92 bridge deck over Drainage Ditch #25 in Louisa County by field investigation and laboratory studies indicates that the primary cause of distress on the structure is corrosion-related damage caused by chloride ingress. Considering that less than five percent of the deck area has had corrosion-related damage after 35 years of service, the structure has performed reasonably well. The two primary design considerations for corrosion protection that contributed considerably and positively to the performance of the bridge deck were adequate concrete cover (2 inches) and the use of galvanized reinforcement for the deck structure. In addition, the bridge has seen slightly lower chloride exposure than some other Iowa bridges examined by WJE, likely related to its low traffic volume.

The field investigation indicated that cracking played a role in causing distress of the deck. Cracks were likely present in the deck shortly after the deck construction. The cracking patterns were largely longitudinally-oriented, and somewhat different than would be encountered on a concrete bridge deck supported on steel girders. The integral deck connection over the piers provides restraint, and the slab was thicker (12 inches) than might be normally present in a deck on steel or concrete girders. Additionally many of the cracks were not through-thickness, and could have been related to concrete settlement over the top reinforcing bars. The longitudinal construction joint may be responsible for additional chloride or moisture ingress and related damage.

Visual, sounding, and GPR surveys were effective in providing information for the assessment. The half-cell potentials obtained were not practical for determination of areas with corroding reinforcing because of the mixing of zinc and steel potentials. However, the half-cell potentials did indicate that the potential for ring-anode effects around repaired areas is high.

The corrosion resistance of the galvanized reinforcing bars has been quantified in terms of paired chloride thresholds and propagation times. Based on this investigation, the corrosion resistance may be best characterized by a chloride threshold of 0.120 percent by weight of concrete and a propagation time of 15 years. However, the paired values representing corrosion resistance may range from a chloride threshold of 0.095 percent by weight with a propagation time of 18 years to a chloride threshold of 0.188 percent by weight of chloride and a propagation time of 5 years. The upper bound of 0.188 percent by weight is likely unconservative, because all bars located identified near this level had active red rust.

These chloride thresholds for galvanized bar represent higher resistance to chloride-induced corrosion than uncoated black bars, which are typically assumed to have a chloride threshold of 0.0350 percent by weight of concrete and a propagation time of 5 years. However, this is somewhat less than the observed chloride thresholds for epoxy-coated bars, for which WJE has previously estimated to range from 0.179 to 0.286 percent by weight of concrete, depending on whether just the top mat or both mats of reinforcing are epoxy-coated. Overall, propagation times for corrosion-related damage appear to be longer for galvanized bars (5 to 18 years) than for uncoated bars (5 years), but still somewhat less than propagation times for epoxy-coated bars (12 to 23 years).

Service life modeling was used to assist in establishing appropriate thresholds and propagation times for the structure and also to estimate the service life extension provided by using galvanized reinforcement instead of uncoated bars. The availability of damage estimates at multiple times over the life of the structure was vital to establishing appropriate thresholds and propagation times for the galvanized reinforcing bars in this structure. Based on this modeling, galvanized reinforcement has provided a service life extension of approximately 22 years compared to uncoated reinforcement.

Galvanized reinforcement has some advantages and disadvantages for use in bridge decks. Apart from an initial build-up of zinc corrosion by-products in the highly-alkaline environment of the fresh concrete, the galvanizing surface did not exhibit signs of deterioration in non-chloride contaminated concrete, suggesting that the level of protection will not degrade with time. Galvanized reinforcement is more tolerant of handling damage than epoxy-coatings on reinforcing bars, due to its harder surface and somewhat reduced sensitivity to damage. However, some precautions should be considered when designing with galvanized reinforcement. Galvanized bars should not be combined with uncoated bars in the same element, because the electrochemical difference in surfaces could cause galvanic corrosion between the types of bars. Galvanized bars will tend to corrode faster than black bars when electrically connected. Additionally, the minimum thickness of galvanized coating should be considered; thicker coatings would be expected to offer greater protection for corrosion of the underlying steel.

As a follow-up to the initial evaluation of the performance of galvanized reinforcing bars, John Lawler of Wiss, Janney, Elstner Associates, Inc. (WJE) visited the project site during deck repair operations, which were performed subsequent to our field investigation of this bridge deck. The deck repair work included milling the top surface of the bridge deck, the removal and replacement of concrete at areas of delamination, casting a concrete overlay over the entire bridge deck, and installing new joints. WJE made site visits on October 7, 2013 and April 2, 2014, in both cases after concrete repair work had begun on one-half of the bridge deck. The objectives of the site visits were to observe repair operations, to inspect the conditions of the bars exposed by the repair process, and to verify that any conditions of distress observed after deck surface milling were consistent with observations of the deck top surface made during the WJE field investigation.

The finding of the follow-up site visits are provided in Appendix E. Most repair openings were generally localized and were directly associated with the corrosion of a single reinforcing bar. The corrosion was generally associated with cracks that were in-line with the corroded bar. The extent of concrete removal was generally consistent with the extent of delaminated concrete identified by WJE during the 2012 field investigation. Further, the increase in damage noted between surveys was determined to fall well within the range of damage projected based on the range of assumed chloride thresholds and propagation times. Therefore, a modification to WJE's quantification of corrosion resistance (ranging from a chloride threshold of 0.095 percent by weight with a propagation time of 18 years to a chloride threshold of 0.188 percent by weight with a propagation time of 5 years) is not warranted based on the new survey information.

6. CONCLUSIONS

This investigation was initiated to assess the corrosion protection provided by galvanized reinforcing bars in the concrete deck of the Iowa State Highway 92 Bridge over Drainage Ditch #25 in Louisa County, which was built in 1976. This work consisted of a field investigation, which included evaluation of existing condition of the deck and material sampling, an extensive laboratory evaluation of the concrete and bar samples obtained, and service life modeling to estimate the level of protection and to provide a basis for comparison with other reinforcing alternatives. The conclusions made based on this investigation are summarized as follows:

- Less than five percent of the deck area has developed corrosion-related damage after 35 years of service in demanding chloride exposure conditions. Surface damage was initially reported in 2006 after 30 years of service.
- State Highway 92 Bridge over Drainage Ditch #25 had slightly lower surface chloride concentrations compared with the other interstate bridges evaluated by WJE in Iowa. Further, the chloride diffusion coefficient of the uncracked concrete was very low.
- The crack affected area of the deck was approximated at 10%, which has a strong influence on the service life of this deck.
- No clear relationship was evident between the bar corrosion and the measured half-cell potentials. Conventional interpretation of half-cell potential measurements were not a good indicator of corrosion activity in the deck.
- The corrosion resistance of the galvanized reinforcing bars has been quantified in terms of paired chloride thresholds and propagation times. Based on this investigation, the corrosion resistance of galvanized reinforcing steel may be best characterized by a chloride threshold of 0.120 percent by weight of concrete and a propagation time of 15 years. However, the paired values representing corrosion resistance may range from a chloride threshold of 0.095 percent by weight with a propagation time of 18 years to an unconservatively high chloride threshold of 0.188 percent by weight of chloride and a propagation time of 5 years. This represents higher resistance to chloride-induced corrosion than typically assumed for uncoated black bars, but is somewhat less than has been observed for epoxy-coated bars during WJE's 2011 Iowa study.
- Based on service life modeling to a damage limit of 5 percent, galvanized reinforcement has provided a life extension of 21 to 27 years compared to what would have been expected for uncoated reinforcement.

7. REFERENCES

Bastidas-Arteaga, E., A. Chateauneuf, M. Sanchez-Silva, Ph. Bressolette, and F. Schoefs. 2011. "A comprehensive probabilistic model of chloride ingress in unsaturated concrete." *Engineering Structures* 33: 720-730.

Bertolini, L., B. Elsener, P. Pedeferri, and R Polder. 2004. *Corrosion of Steel in Concrete: Prevention, Diagnosis, Repair.* Germany: Wiley-VCH.

Broomfield, John P. 2007. *Corrosion of Steel in Concrete.* New York: Taylor and Francis.

Chapra, S. C., and R. P. Canale. 2002. *Numerical Methods for Engineers.* 4th. McGraw-Hill.

Krauss, P. D., J. S. Lawler, and K. A. Steiner. 2009. *Guidelines for Selection of Bridge Deck Overlays, Sealers, and Treatments, NCHRP Project 20-07, Task 234.* Washington, D.C.: National Cooperative Highway Research Program.

Lee, S.K., and P.D. Krauss. 2003. *Service Life Extension of Northern Bridge Decks Containing Epoxy-Coated Reinforcing Bars.* Northbrook, IL: Wiss, Janney, Elstner Associates, Inc.

Liu, Y., and R. Weyers. 1998. "Modeling the Time-to-Corrosion Cracking in Chloride Contaminated Reinforced Concrete Structures." *ACI Materials Journal* 95 (6): 675-681.

Sagüés, A.A. 2003. "Modeling the Effects of Corrosion on the Lifetime of Extended Reinforced Concrete Structures." *Corrosion* 854-866.

Vu, K., M. Stewart, and J. Mullard. 2005. "Corrosion-Induced Cracking: Experimental Data and Predictive Models." *ACI Structural Journal* 102 (5): 719-726.

Wiss, Janney, Elstner Associates, Inc. 2011. "Performance Evaluation of Iowa Bridge Decks Constructed with Epoxy-Coated Reinforcing Bars." Northbrook.

Wyss, G. D., and K. H. Jorgenson. 1998. "A User's Guide to LHS: Sandia's Latin Hypercube Sampling Software." Risk Assessment and Systems Modeling Department, Sandia National Laboratories, Albuquerque.

Yeomans, Stephen R., ed. 2004. *Galvanized Steel Reinforcement in Concrete.* Elsevier.

Tables

Table 3.1. Observed Distress

Item	Quantity
Cracks noted in 2012	279.5 lin. ft.
Patch repairs performed in 2009	322.0 sq. ft.
New distress noted in 2012	48.5 sq. ft.

Table 3.2. History of Distress

Item	Date	Quantity	Damage Area[2] (%)
Distress noted by IaDOT field survey	2006	21.0 sq. ft.	0.7
Estimated distress at time of repair[1]	2009	79.0 sq. ft.	2.5
Total distress (estimated distress[1] plus distress observed in 2012)	2012	127.5 sq. ft.	4.1

[1] The distress associated with the 2009 repairs was estimated by drawing hypothetical distress areas within the individual repairs, as shown in Figure A.1 in Appendix A.
[2] Excludes repair at temporary barrier rail.

Table 3.3. Concrete Cover Measured by GPR

Parameter	Westbound Lane and Shoulder	Eastbound Lane and Shoulder
Average (in.)	2.20	2.30
Std. dev. (in.)	0.17	0.24
Minimum (in.)	1.64	1.72
Maximum (in.)	2.79	3.02
Number of readings	390	363

Table 3.4. Description of Cores

Core ID	Lane Direction	Location in lane [1]	Station, ft[2]	Distance to Edge Barrier	Feature	Core length, in.	Top bar diameter, in.	Top bar cover, in.	Vertical crack?	Delamination Observed?
1	WB	CWP	3	18'-0"	5 in. off const. jt.	7	1 1/4	2 1/4	No	Yes
2	WB	Shoulder	7	5'-6"	8 in. from edge of marked delamination	6 1/4	1 1/4	2 3/8	Yes	Yes [3]
3	WB	Shoulder	30	5'-6"	—	7 1/2	7/8	2 1/4	No	No
4	WB	LWP	40	20'-0"	—	7	7/8	2	No	No
5	WB	CWP	56	18'-0"	5 in. off const. jt. and crack	7 1/4	1 1/4	2 3/4	Yes	Yes
6	WB	Shoulder (edge)	60	1'-3"	—	8 1/4	1 1/4	2	No	No
7	EB	RWP	28	12'-0"	—	7 3/8	1 1/4	2 1/4	No	No
8	EB	Shoulder	37.5	4'-0"	—	8 1/4	7/8	3 1/4	No	No
9	EB	RWP	58	12'-0"	—	8 3/8	1 1/4	2 7/8	Yes	Yes
10	EB	Shoulder	24	8'-0"	—	5 1/2	1 1/4	1 7/8	Yes	Yes

[1]. RWP = right wheel path; LWP: left wheel path; CWP: between wheel paths
[2]. Station marked from west end of bridge
[3]. Delamination observed in core after extraction; delamination was not identified by sounding prior to coring.

Table 3.5. Acid-Soluble Chloride Contents by Core

Core	Acid-Soluble Chloride Test Results						
1	Depth, in.	--	--	--	2.24	--
	Chloride, % by wt. conc.	--	--	--	0.266	--
2	Depth, in.	--	--	--	1.98	--
	Chloride, % by wt. conc.	--	--	--	0.193	--
3	Depth, in.	0.20	0.70	1.27	2.06	--
	Chloride, % by wt. conc.	0.340	0.284	0.144	0.050	--
4	Depth, in.	0.07	0.67	1.13	2.60	6.22
	Chloride, % by wt. conc.	0.307	0.219	0.132	0.001	0.003
5	Depth, in.	0.30	0.74	1.17	2.11	--
	Chloride, % by wt. conc.	0.536	0.438	0.368	0.256	--
6	Depth, in.	0.27	0.48	1.01	2.12	--
	Chloride, % by wt. conc.	0.149	0.088	0.032	0.005	--
7	Depth, in.	--	--	--	2.26	--
	Chloride, % by wt. conc.	--	--	--	0.084	--
8	Depth, in.	0.30	0.79	1.31	3.20	--
	Chloride, % by wt. conc.	0.355	0.319	0.199	0.004	--
9	Depth, in.	0.23	0.72	1.21	2.70	--
	Chloride, % by wt. conc.	0.499	0.454	0.341	0.193	--
10	Depth, in.	--	--	--	1.67	--
	Chloride, % by wt. conc.	--	--	--	0.376	--

Table 3.6. Observed Corrosion on Extracted Bars

Core ID	Surface	Red Corrosion Product (%)	White Corrosion Product (%)	Overall Corrosion Severity
1	Top	40	50	Light/Moderate
	Bottom	0	50	Light
2	Top	50	30	Moderate/Heavy
	Bottom	5	60	Light
3	Top	0	0	None
	Bottom	0	10	Light
4	Top	0	0	None
	Bottom	0	10	Light
5	Top	30	30	Moderate
	Bottom	5	70	Light
6	Top	0	0	None
	Bottom	0	0	None
7	Top	0	0	None
	Bottom	0	20	Light
8	Top	5	0	Light
	Bottom	0	50	Light
9	Top	95	5	Heavy
	Bottom	45	40	Moderate/Heavy
10	Top	75	25	Heavy
	Bottom	10	85	Moderate/Heavy

Table 4.1. Exposure, Concrete, and Geometry Parameters for Service Life Model

Parameter	Distribution	Mean	COV (%)
C_s (% by wt. conc.)	Normal	0.416	32
D_a, uncracked (in.^{2}/yr.)	Normal	0.036	29
D_a, cracked	Normal	0.118	11
Cover (in.)	Lognormal	2.249	9.4
Crack-affected area (%)	--	10	--

Table 4.2. Corrosion Threshold, Propagation Times, and Expected Service Life

Reinforcement Type	Corrosion Threshold, % by wt. conc.	Propagation Time (yrs)	Expected age at 5 percent damage	Expected age at 10 percent damage	Service Life extension over uncoated bars (5 percent damage)	Service Life extension over uncoated bars (10 percent damage)
Uncoated	0.035	5	14	18	--	--
Galvanized	0.095	18	35	42	21	25
	0.120	15	36	45	22	28
	0.188	5	41	56	27	38
Epoxy-coated	0.180	12	46	> 60	32	> 42
	0.180	23	58	> 60	44	> 44

Figures

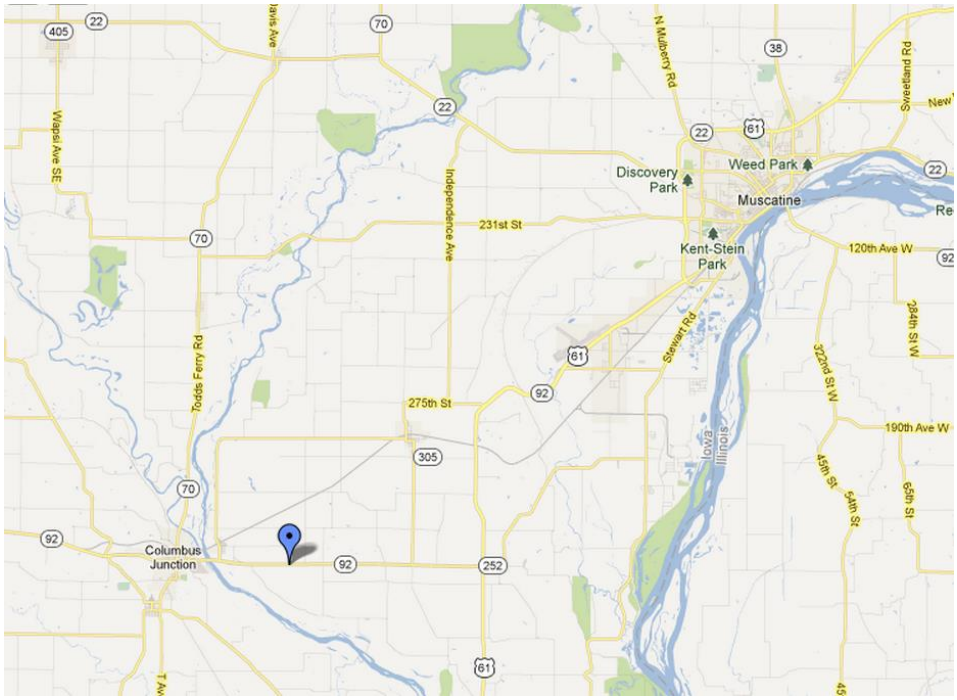

Figure 1.1. Location (blue marker) of Iowa State Highway 92 bridge across Drainage Ditch #25 in Louisa County, Iowa (Structure No. 5854.5S092)

Figure 1.2. South elevation of subject bridge.

Figure 2.1. Measuring reinforcing cover depth with GPR.

Figure 2.2. Drilling a core sample from the deck.

Figure 2.3. Measuring half-cell potentials with single rolling wheel equipment (Proceq Canin+).

Figure 2.4. Measuring half-cell potentials with the nine-cell rolling test frame.

Figure 3.1. Overall view of eastbound lane of bridge, looking east. Chalk lines indicate cracks and delaminations identified by survey.

Figure 3.2. Overall view of westbound lane of bridge, looking east. Chalk lines indicate cracks and delaminations identified by survey.

Figure 3.3. Patched rail anchor hole at west end of westbound lanes.

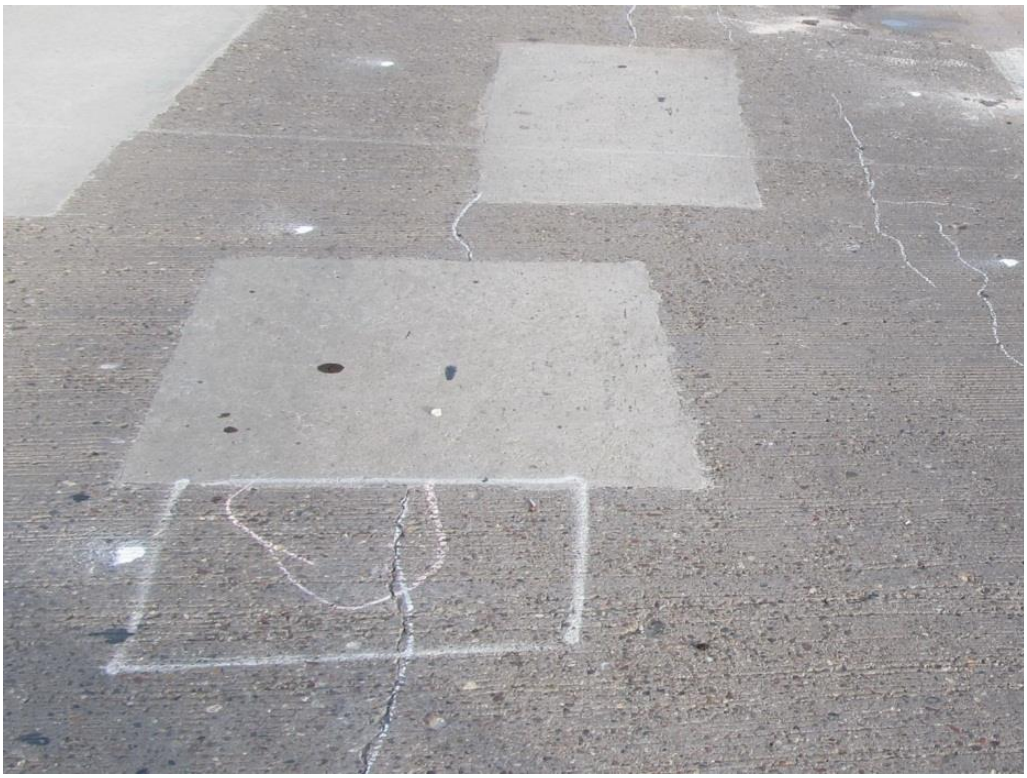

Figure 3.4. Delamination marked in pink chalk and proposed repair location marked in white paint adjacent to previous patch repair.

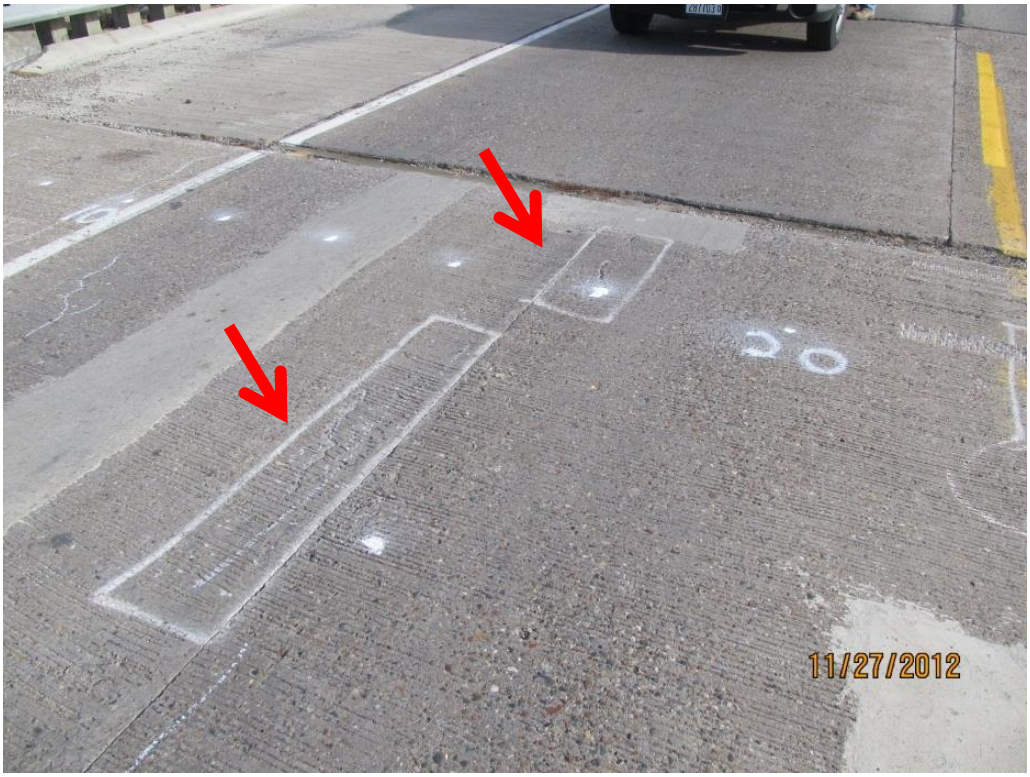

Figure 3.5. Repair areas marked by IaDOT associated with cracking adjacent to construction joint, but not identified as delaminated.

Figure 3.6. Deck underside east span.

Figure 3.7. Deck underside center span.

Figure 3.8. Moisture staining on deck underside surrounding drain penetration.

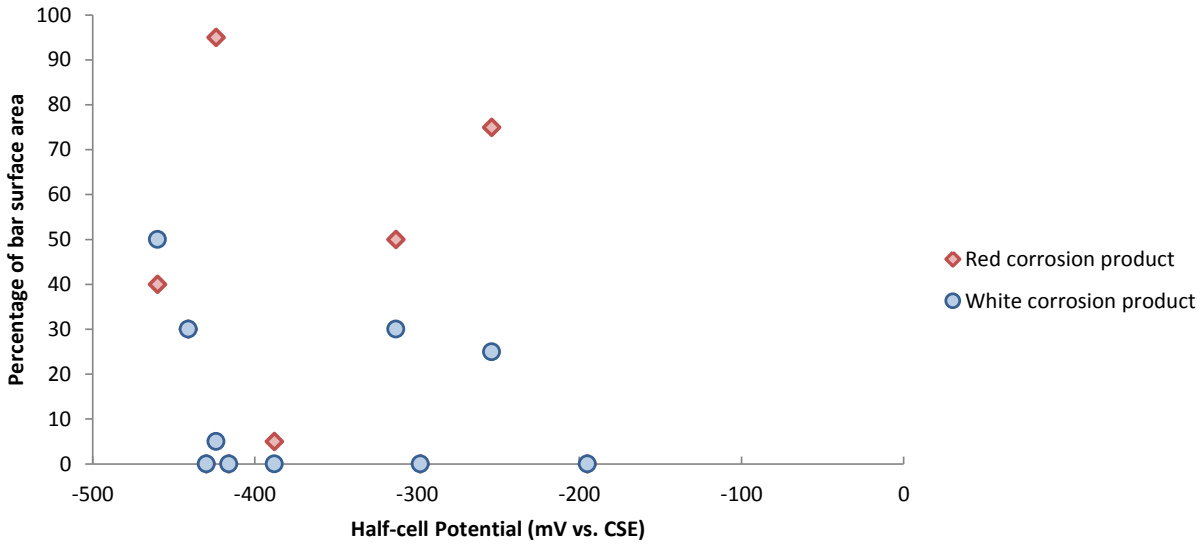

Figure 3.9. Relationship of half-cell potential to corrosion product observed on extracted bar sample.

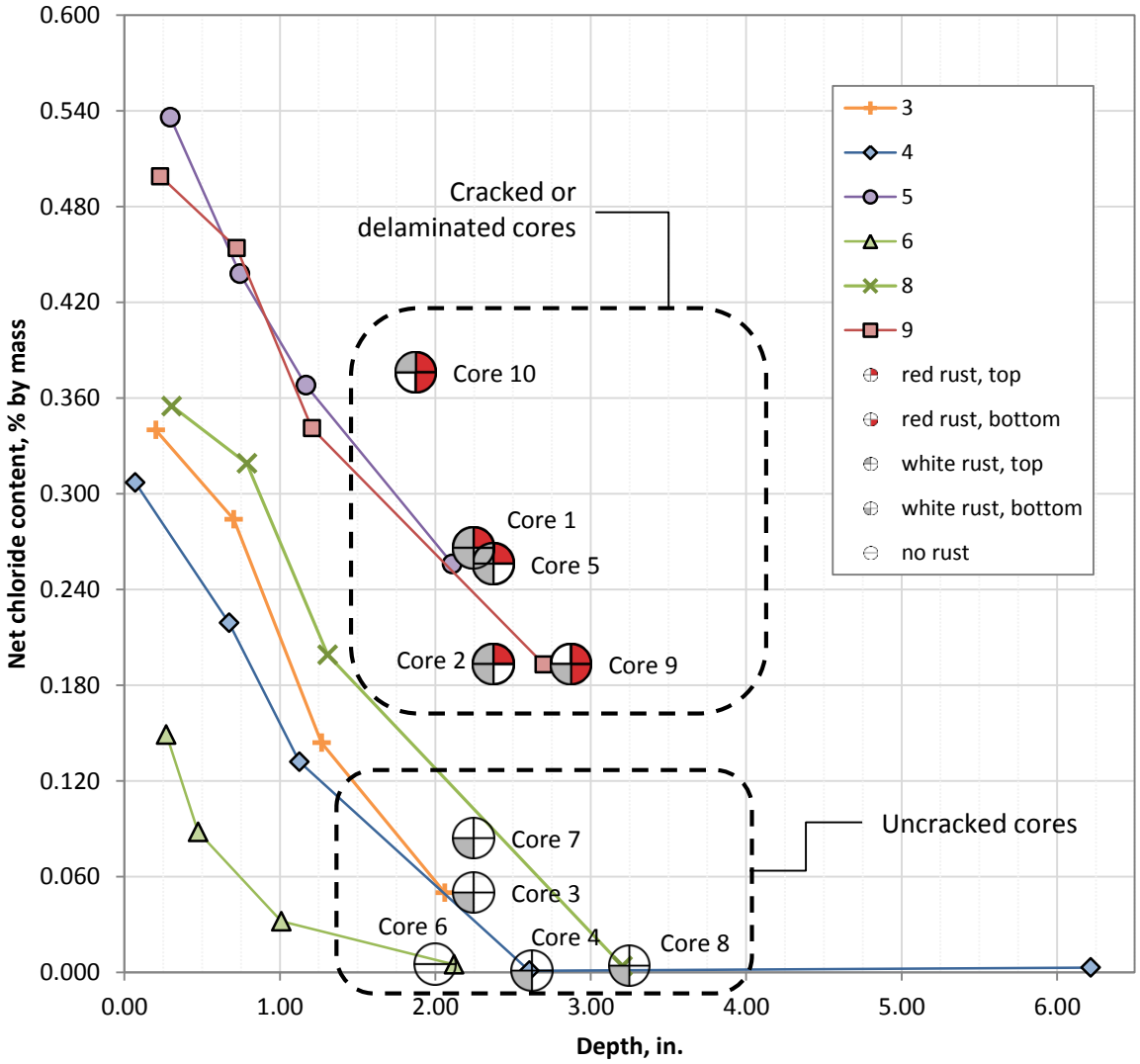

Figure 3.10. Chloride content profiles with depth for 6 cores. Chloride content at bar depth is also shown for all 10 cores. The corrosion state of extracted bars is indicated by the symbol shown for each core, where a colored indication (grey or red) denotes that 10 percent or more of the bar exhibited white or red rust. Lines for the chloride profiles do not pass exactly through the bar designation for each core, because the actual position of the slice varied slightly relative to the top of the bar.

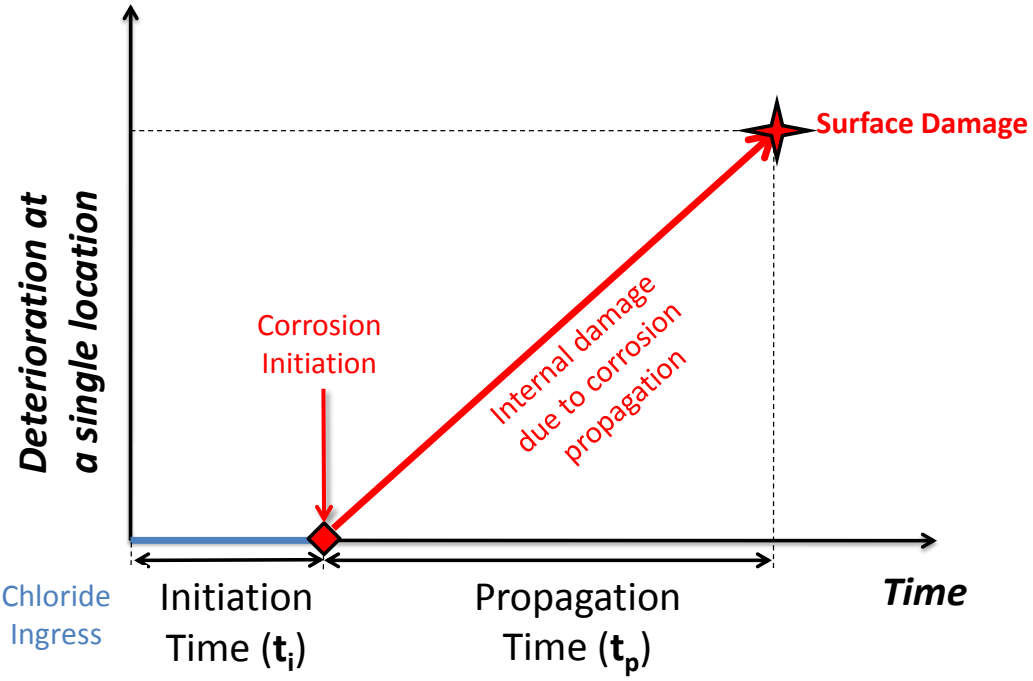

Figure 4.1.Corrosion sequence (adapted from Tuutti 1982).

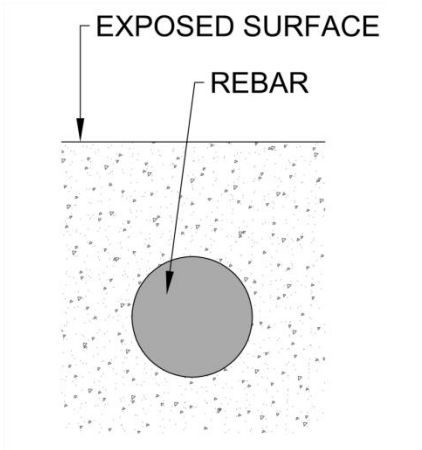

Step 1: New construction

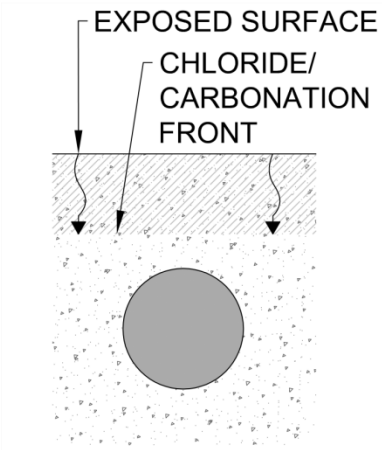

Step 2: Ingress begins

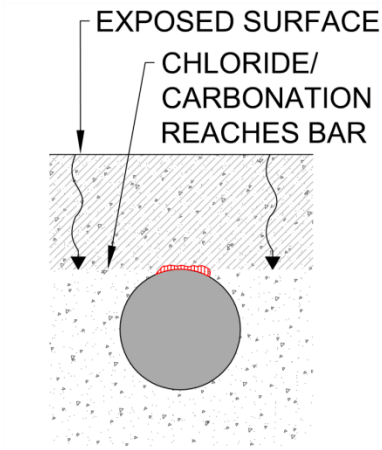

Step 3: Ingress reaches bar and corrosion initiates

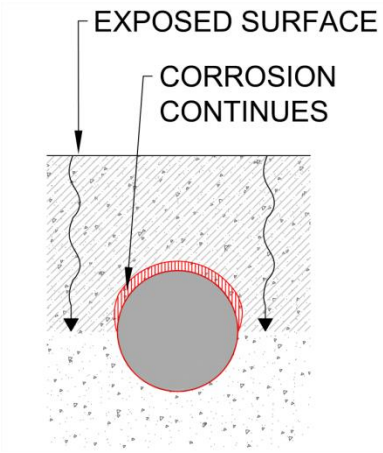

Step 4: Corrosion continues and causes internal damage

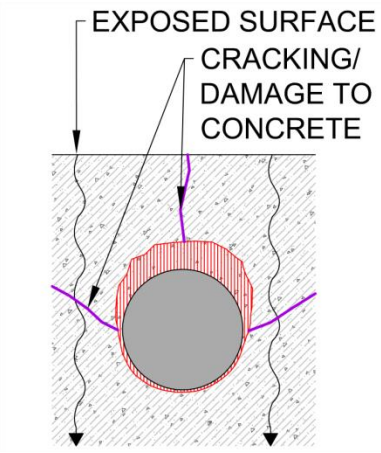

Step 5: Corrosion continues and causes surface damage

Figure 4.2. Illustration of corrosion sequence.

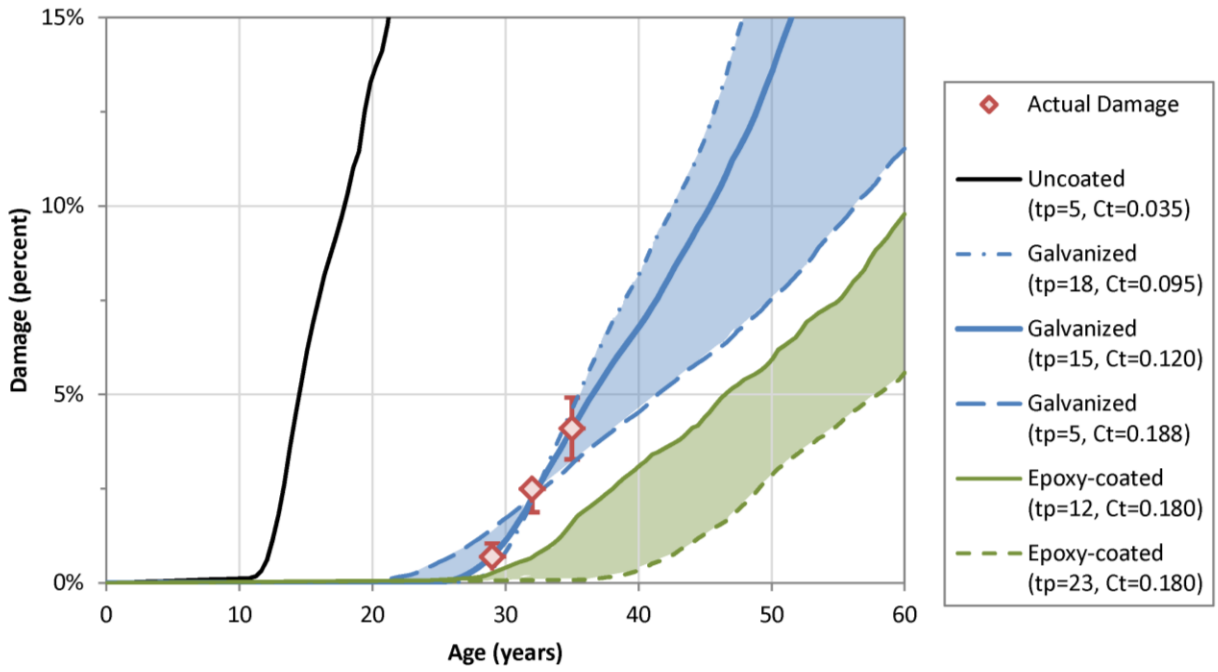

Figure 4.3. Results of service life model for bridge. (Propagation time (t_p) is given in years, and chloride threshold (c_t)is given in percent by weight of concrete.)

WJE ENGINEERS ARCHITECTS MATERIALS SCIENTISTS

APPENDIX A

Visual, Sounding, and Half-Cell Potential Plans

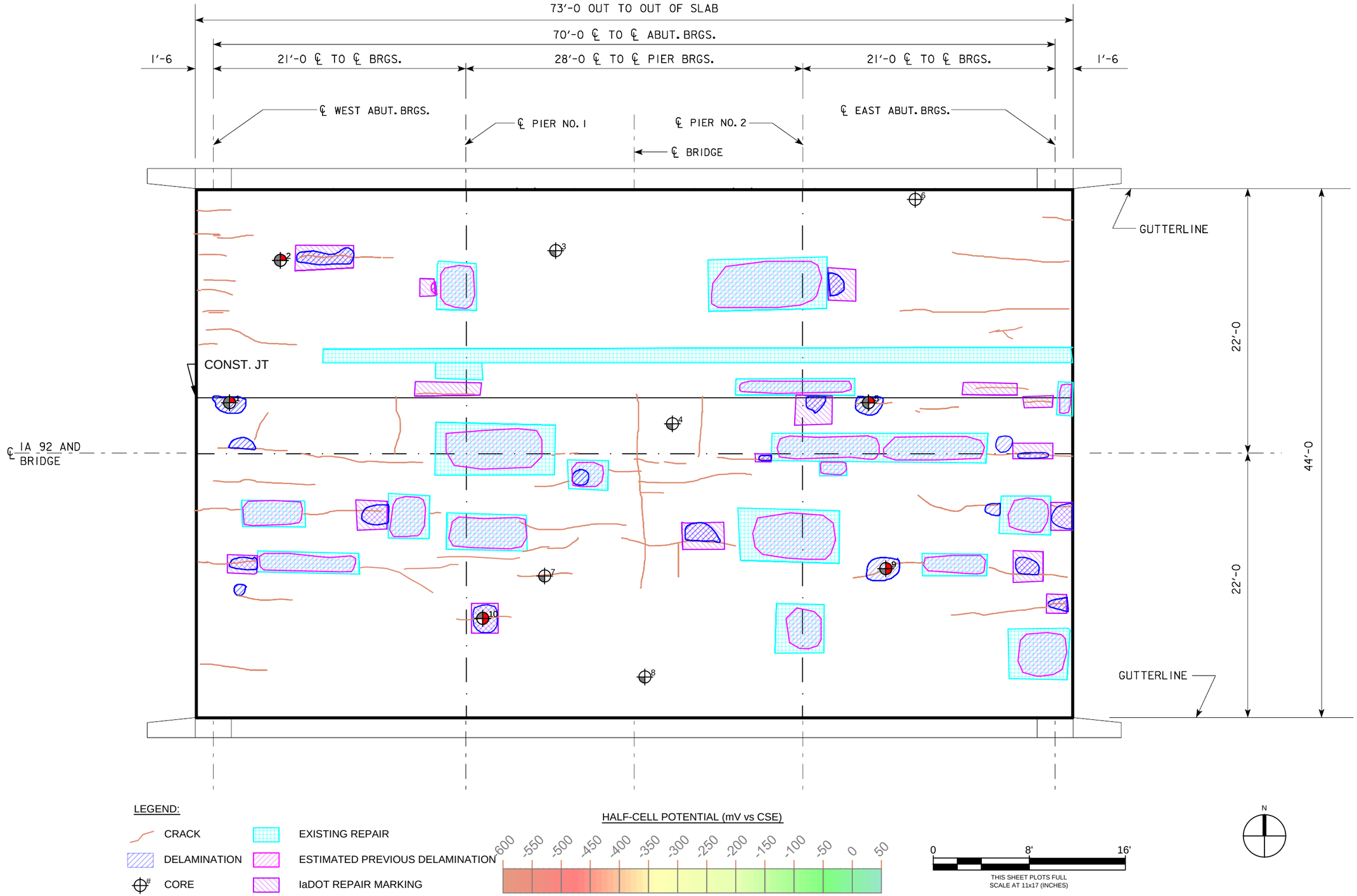
73'-0 OUT TO OUT OF SLAB
70'-0 ℄ TO ℄ ABUT. BRGS.
1'-6
21'-0 ℄ TO ℄ BRGS.
28'-0 ℄ TO ℄ PIER BRGS.
21'-0 ℄ TO ℄ BRGS.
1'-6
℄ WEST ABUT. BRGS.
℄ PIER NO. 1
℄ PIER NO. 2
℄ EAST ABUT. BRGS.
℄ BRIDGE
GUTTERLINE
CONST. JT
℄ IA 92 AND BRIDGE
22'-0
44'-0
22'-0
GUTTERLINE
1
2
3
4
5
6
7
8
9
10
LEGEND:
CRACK
DELAMINATION
CORE
EXISTING REPAIR
ESTIMATED PREVIOUS DELAMINATION
IaDOT REPAIR MARKING
HALF-CELL POTENTIAL (mV vs CSE)
-600 -550 -500 -450 -400 -350 -300 -250 -200 -150 -100 -50 0 50
0
8'
16'
THIS SHEET PLOTS FULL SCALE AT 11x17 (INCHES)
N

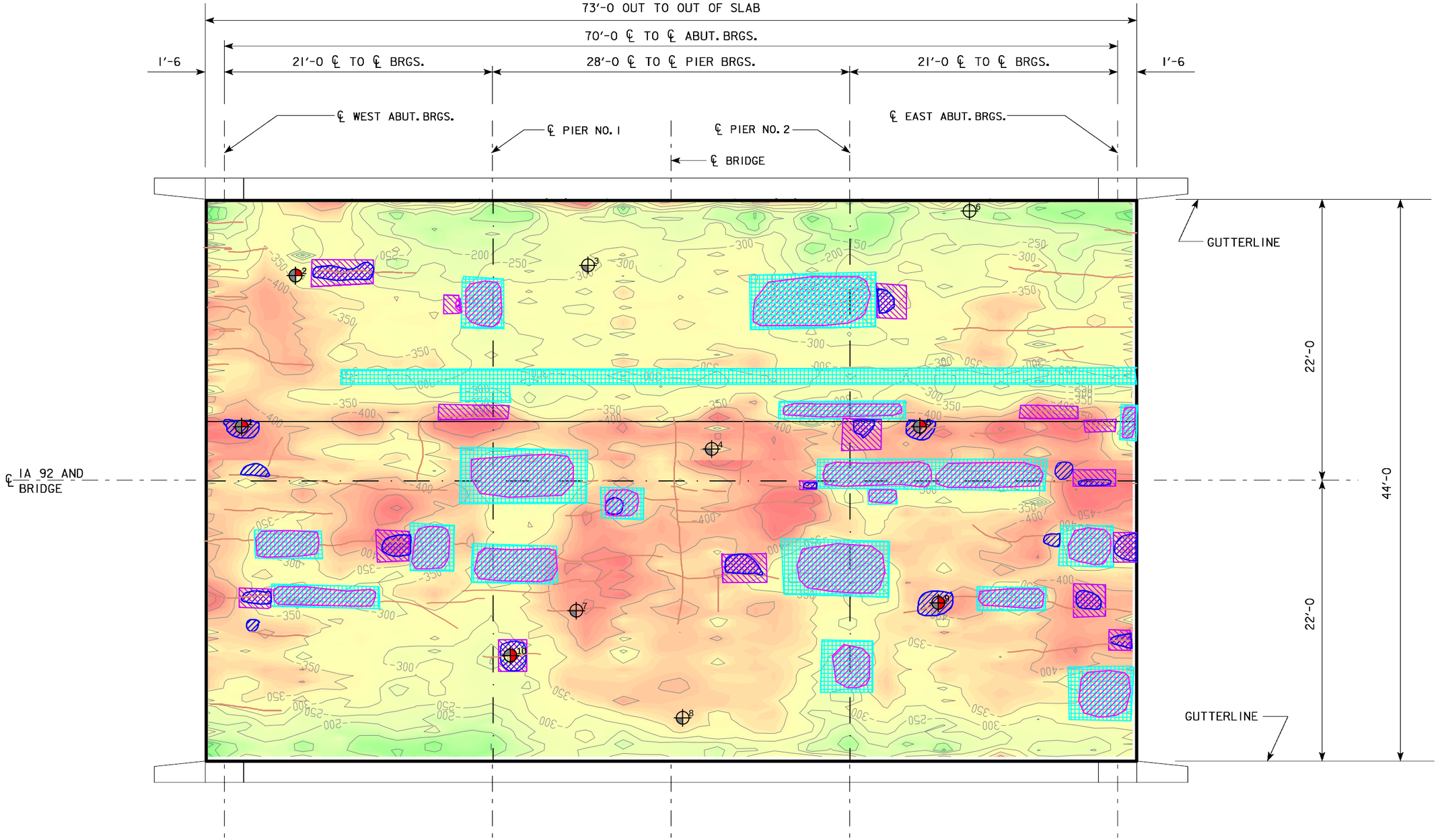

WJE ENGINEERS ARCHITECTS MATERIAL SCIENTISTS

Wiss, Janney, Elstner Associates, Inc.

Iowa 92 Galvanized Reinforcing Bridge

WJE No. 2012.5759

November 27, 2012

Figure A.2

HCP using Canin+

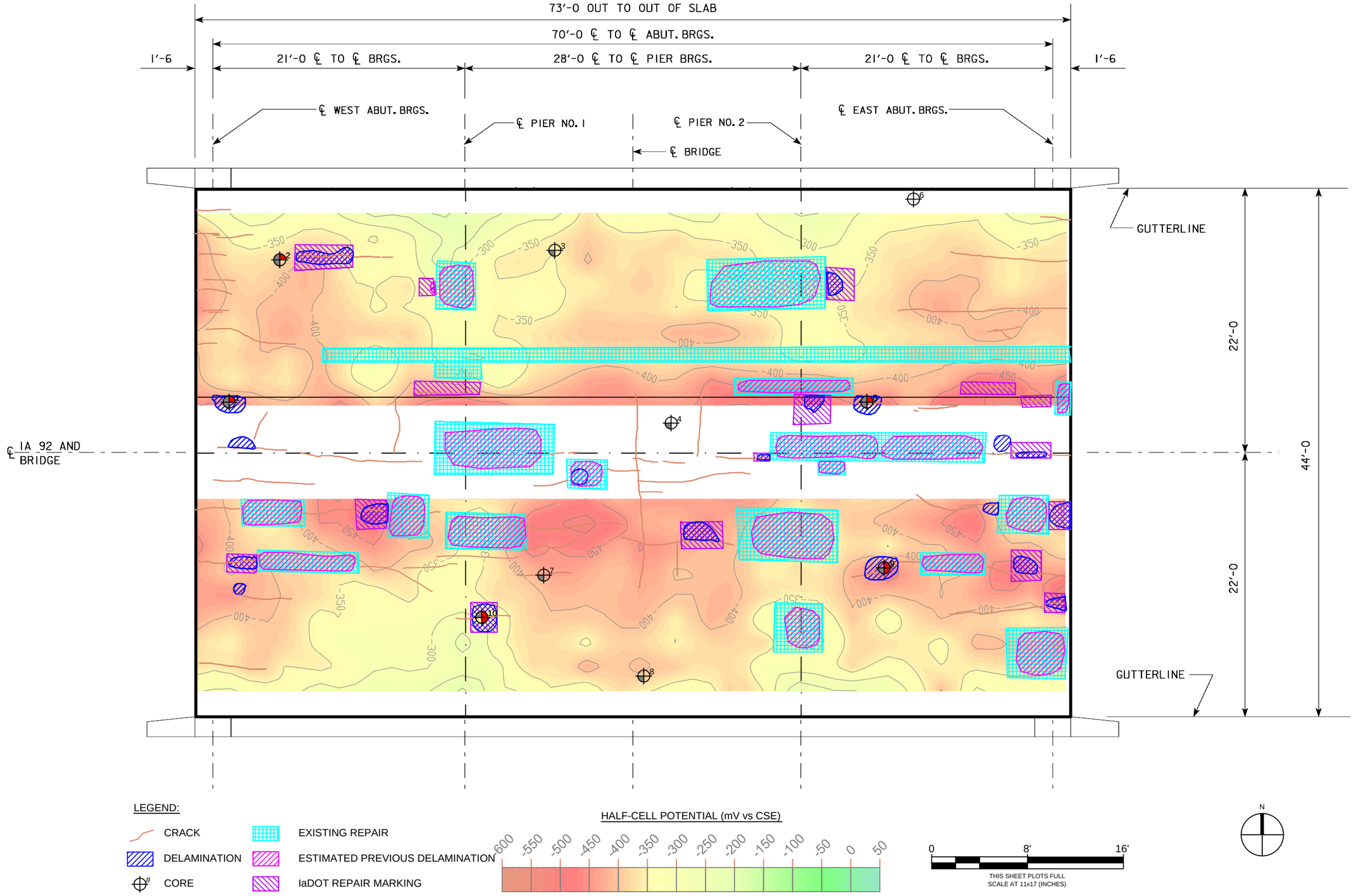
73'-0 OUT TO OUT OF SLAB
70'-0 ℄ TO ℄ ABUT. BRGS.
1'-6
21'-0 ℄ TO ℄ BRGS.
28'-0 ℄ TO ℄ PIER BRGS.
21'-0 ℄ TO ℄ BRGS.
1'-6
℄ WEST ABUT. BRGS.
℄ PIER NO. 1
℄ PIER NO. 2
℄ EAST ABUT. BRGS.
℄ BRIDGE
GUTTERLINE
22'-0
44'-0
℄ IA 92 AND BRIDGE
GUTTERLINE
LEGEND:
CRACK
DELAMINATION
CORE
EXISTING REPAIR
ESTIMATED PREVIOUS DELAMINATION
IaDOT REPAIR MARKING
HALF-CELL POTENTIAL (mV vs CSE)
-600 -550 -500 -450 -400 -350 -300 -250 -200 -150 -100 -50 0 50
0 8' 16'
THIS SHEET PLOTS FULL SCALE AT 11x17 (INCHES)
N

WJE ENGINEERS ARCHITECTS MATERIALS SCIENTISTS

APPENDIX B

Core Sample Photographs

Figure 1. Photographs of Core 1.

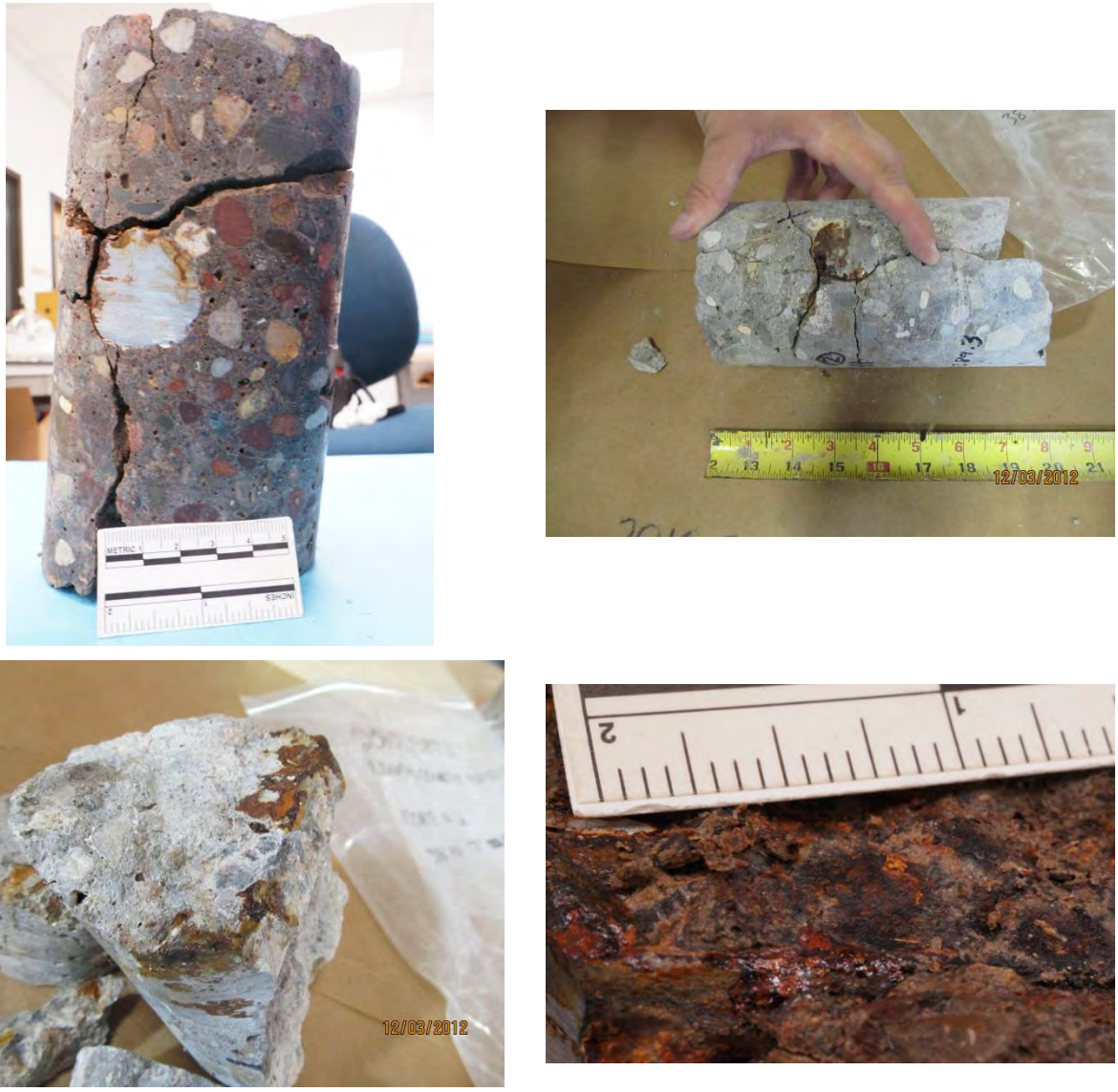

Figure 2. Photographs of Core 2.

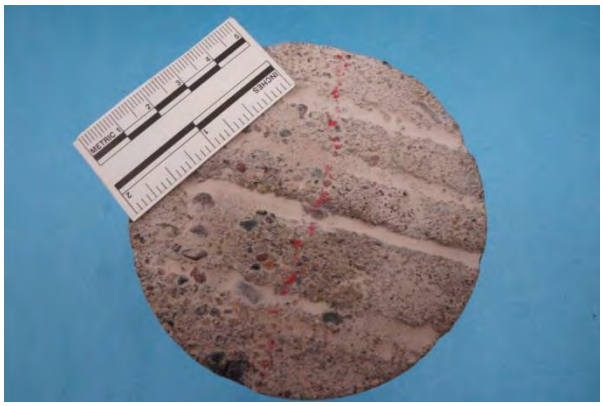

Figure 3. Photographs of Core 3.

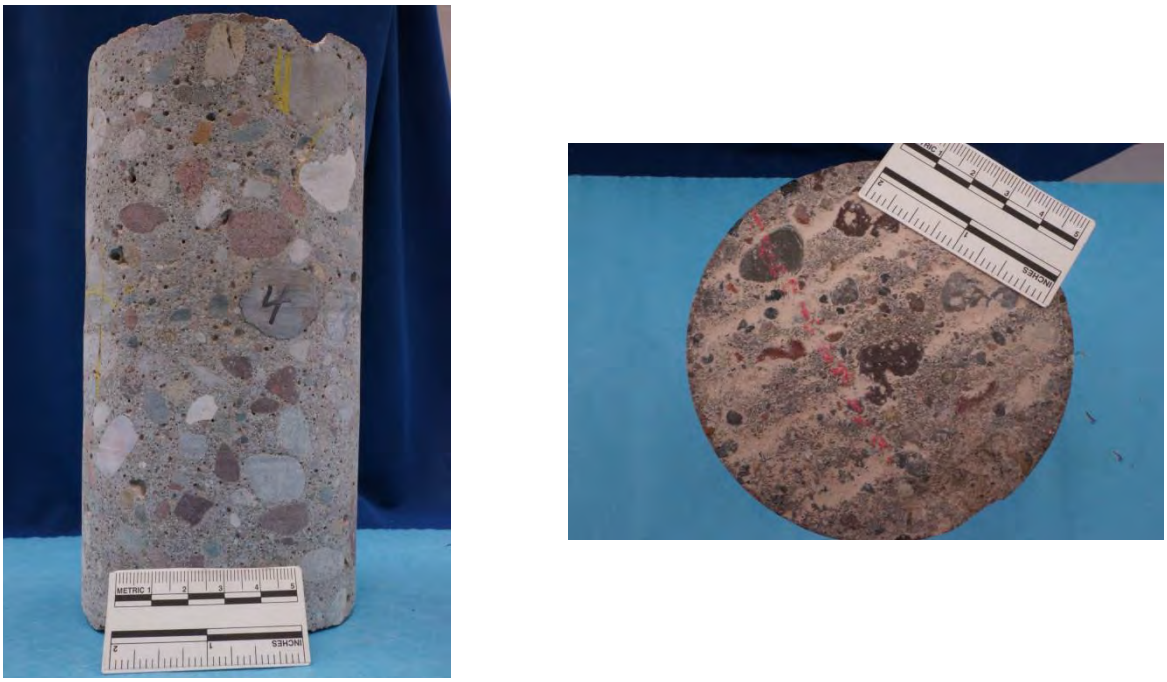

Figure 4. Photographs of Core 4.

Figure 5. Photographs of Core 5.

Figure 6. Photographs of Core 6.

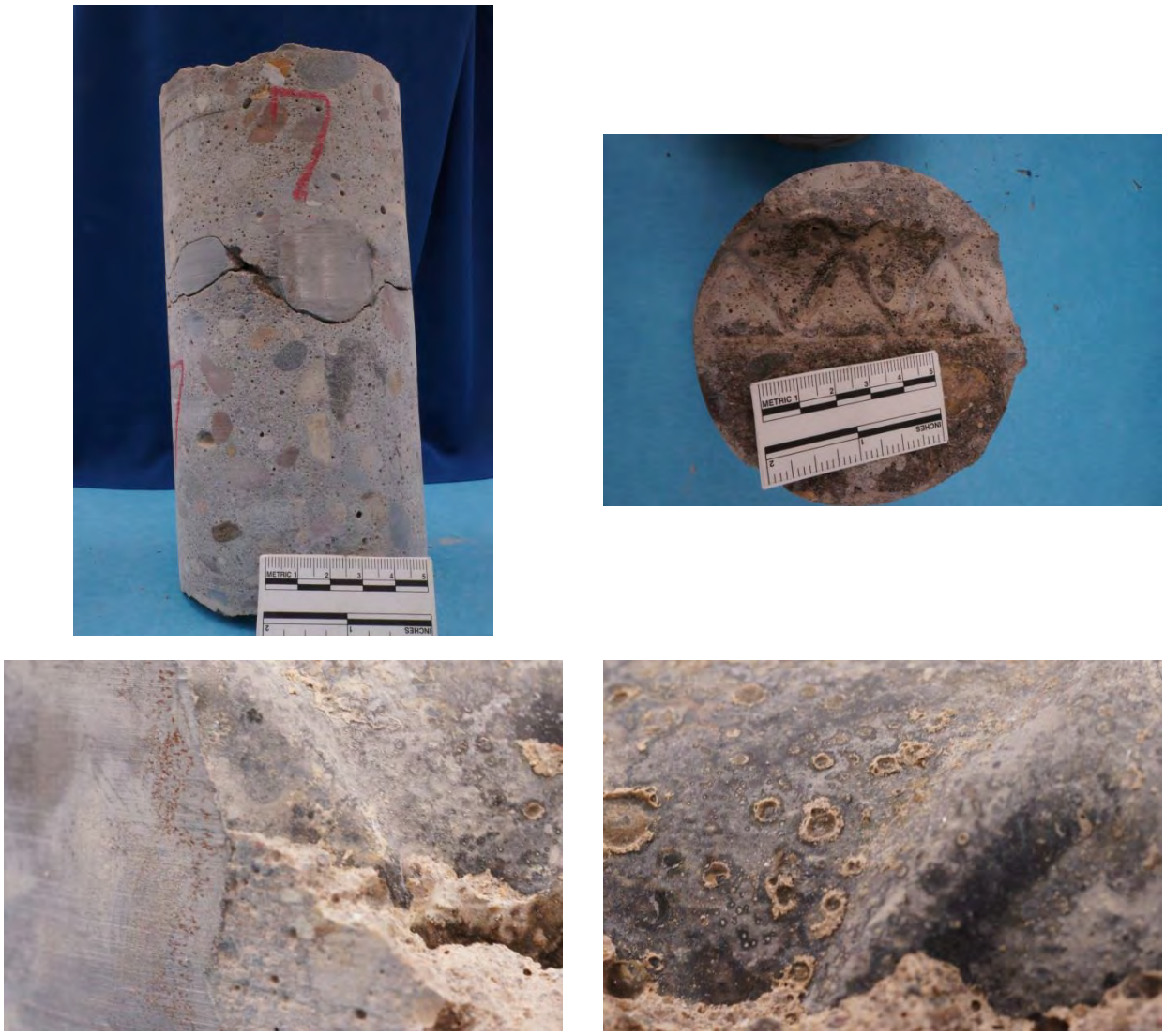

Figure 7. Photographs of Core 7.

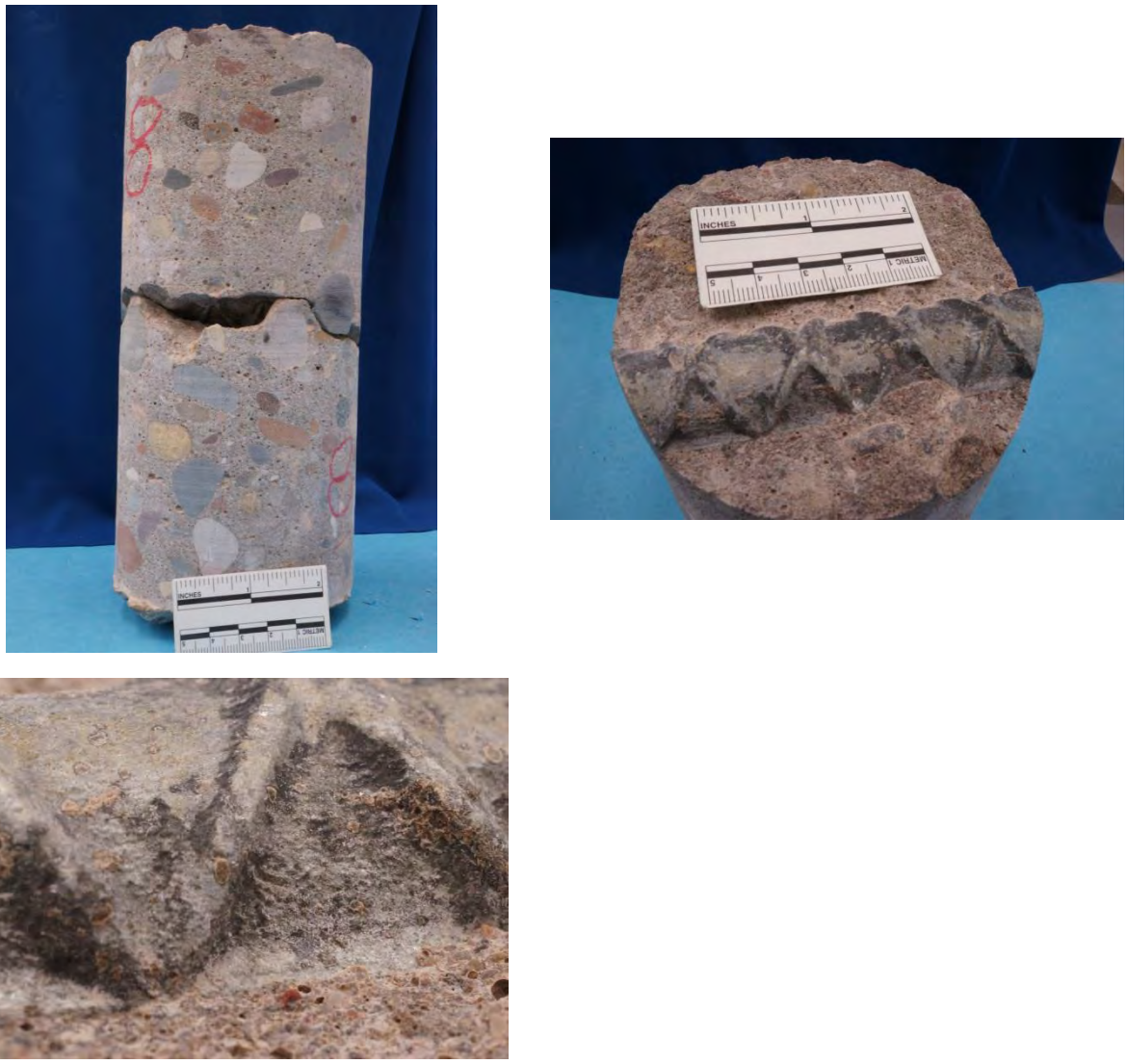

Figure 8. Photographs of Core 8.

Figure 9. Photographs of Core 9.

Figure 10. Photographs of Core 10.

WJE ENGINEERS ARCHITECTS MATERIALS SCIENTISTS

APPENDIX C

Petrographic Examination

WJE ENGINEERS ARCHITECTS MATERIALS SCIENTISTS

Wiss, Janney, Elstner Associates, Inc.
330 Pfingsten Road
Northbrook, Illinois 60062
847.272.7400 tel | 847.291.5189 fax
www.wje.com

INTEROFFICE MEMORANDUM

Via: Project Folder

To: Paul Krauss

From: Uznanski, Lidia L.

Date: February 22, 2013

Project: Iowa State Highway 92 Over Drainage Ditch #25
WJE No. 2012.5759

Subject: Concrete Petrography

PETROGRAPHIC STUDIES OF CONCRETE

Petrographic examination of concrete samples provides useful information on the concrete constituents and durability. Core 8 was examined petrographically using methods of ASTM C856, "*Standard Practice for Petrographic Examination of Hardened Concrete*." The examination was performed using stereoscopic and petrographic microscopes at magnifications ranging from 10x to 600x. Powder mounts were employed in the examination using the polarized-light microscope. The examined sections of the core include top 3-inch and the bottom 3-1/2-inch sections of the core. Horizontal slices had been removed from mid-depth of the core for chloride analyses prior to receiving the sample for petrographic studies.

Additionally, the top regions of six cores were tested for the depths of carbonation of the cement paste. The measured depths of carbonation are provided in Table 1. This testing could not be conducted on four other cores because the top sections of those cores were consumed in other testing.

Core 8

Condition - The top surface of the concrete exhibits rake marks. The top surface is slightly weathered and somewhat uneven. A few aggregate particles have been dislodged from the top surface of the concrete. The concrete mix appears uniform and well consolidated throughout the core sample. The lower section of the core contains an impression of a reinforcing bar. (Figure 1). Corrosion staining was not observed.

A few fine microcarcks were detected on the lapped surfaces of the sample (Figures 1, 2, and 3). One microcrack slopes at an angle from the top surface and exits from the side of the core at the depth of 3/4 inch. It splits into a few finer microcracks just below the top surface. The second main microcrack is found in the bottom section of the core. This microcrack extends from the cut, bottom surface mostly through the section, terminating approximately 1/4 inch below the top of that section. The microcrack appears slightly wider near the cut (bottom) surface than near the fractured/cracked (top) surface. Both microcracks mainly pass around aggregate particles. Impression of a rebar is visible in the middle section

of the core. The widths of the microcracks are 1 mil or less. The microcrack in the top region of the concrete may be shrinkage/carbonation-related, and the microcrack in the lower region of the core could also be related to shrinkage or it could be due to flexural stress.

Small amounts of secondary mineral deposits, mainly calcium hydroxide, some ettringite, and possibly deicing salts, were detected inside some air-voids only in the top ¼ inch of the concrete (Fig.4). This suggests that the concrete from this particular area is moderately dense or was not subjected to a lot of moisture.

Aggregate - Coarse aggregate represents siliceous and calcareous gravel having maximum nominal size of 3/4 inch. It is composed of variety of rock types that include granite, limestone, volcanic rocks, quartzite, sandstone, siltstone, chert, and small amounts of other rocks. Some of the sedimentary rocks, sandstone and siltstone, are somewhat soft and absorbent, but there is no indication of problems associated with those particles within the concrete. The chert particles occur in two forms; hard and dense, and somewhat soft and porous. Some of the chert particles exhibit reaction rims as observed on the lapped surfaces of the core. However, there is no indication of alkali-silica reaction (ASR); secondary deposits of silica gel were not detected. Fine aggregate is natural siliceous sand composed mainly of quartz and small amounts of igneous rocks. The aggregate is well graded and uniformly distributed within the concrete. The total aggregate content appears somewhat lower than in average concrete, resulting in slightly higher content of the cement paste estimated at 30 percent by volume. The aggregate particles are well bonded to the cement paste.

Paste - The cement paste is moderately hard to hard and moderately dense. The estimated cement content is 6 to 7 bags per cubic yard of concrete. The water cement ratio is overall relatively low, estimated to range from 0.38 to 0.45; some variability were detected on a micro-scale. Hydration of the cement is moderately advanced to advanced and normal. Pozzolans were not detected within the mix. The depth of carbonation of the cement paste ranges from 1/16 to 1/8 inch as measured from the top surface of the core.

Air - The concrete is air-entrained. The approximate air content is 6.5 to 7 percent. The air occurs mainly as small and medium size, spherical voids that are typical of entrained air, and a small number of medium size, irregularly shaped voids typical of entrapped air. The distribution of the air voids is generally uniform. The air voids are somewhat less frequent within the top 1/4 inch of the core.

Summary of Petrographic Studies

The petrographic examination of Core 8 indicates that the concrete mix contains siliceous and calcareous gravel coarse aggregate and natural siliceous sand fine aggregate. The cement paste is strong and of good quality. The estimated water-cement ratio is 0.38 to 0.45, and the approximate cement content is 6 to 7 bags per cubic yard of concrete. Pozzolans were not detected. The concrete is air entrained and contains 6.5 to 7 percent air. The air void system is of good quality and is judged to be adequate for proper protection of the concrete from possible cyclic freeze-thaw damage.

A few longitudinal microcracks were detected within the concrete. Two main microcracks included one in the top 3/4 inch of the core and one in the bottom 3 inches of the core. The microcracks are very fine with widths measuring 1 mil or less, and mainly pass around aggregate particles. These microcracks may be

related to shrinkage and flexing of the slab. The tiny microcracks branching off the main microcracks near the very top of the core most likely are related to carbonation shrinkage of the cement paste.

Small amounts of secondary mineral deposits were detected inside air voids along top surface of the concrete. The scarcity of the secondary deposits indicates that the concrete remained relatively dry or impermeable while in service. There was no evidence of ASR associated with chert particles present within the aggregate.

Storage: Thirty days after completion of our studies, the samples will be discarded unless the client submits a written request for their return. Shipping and handling fees will be assessed for any samples returned to the client. Any hazardous materials that may have been submitted for study will be returned to the client and shipping and handling fees will apply. The client may request that WJE retain samples in storage in our warehouse. In that case, a yearly storage fee will apply.

Table 1 - Depths of carbonation of the cement paste

Core ID	Depth of paste carbonation from exposed surface (inch)
1.	1/8 to 1/4
2.	1/16 to 1/8
3.	1/8 to 1-1/4 (carbonation might partially coincide with pre-existing microcrack)
7.	1/4
8.	1/16 to 1/8
10	1/8 to 1/4

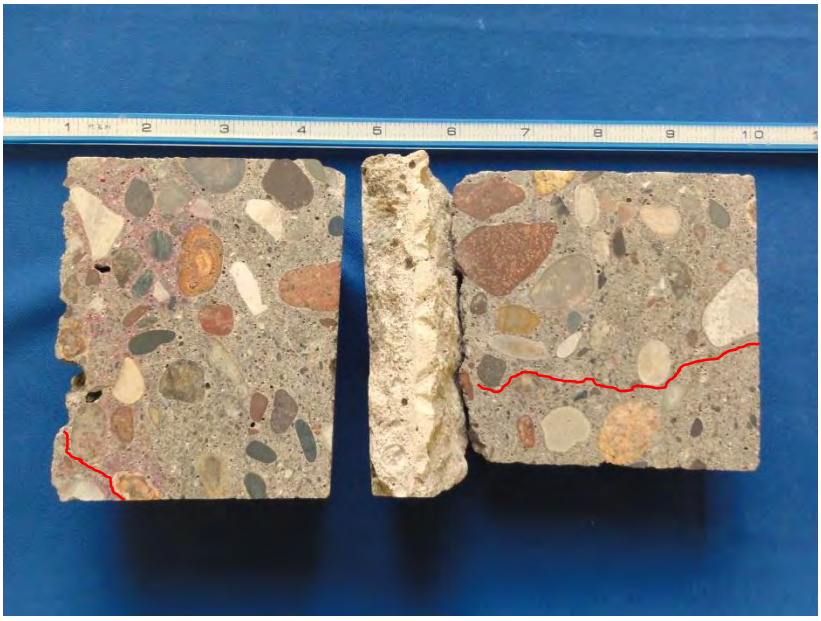

Figure 1. Sections of Core 8; top surface of the concrete is on the left of the photograph. The locations of the microcracks are outlined in red. Impression of a rebar is visible in the middle section of the core. Similar impression (not visible in photo) is also present at the top of the bottom section.

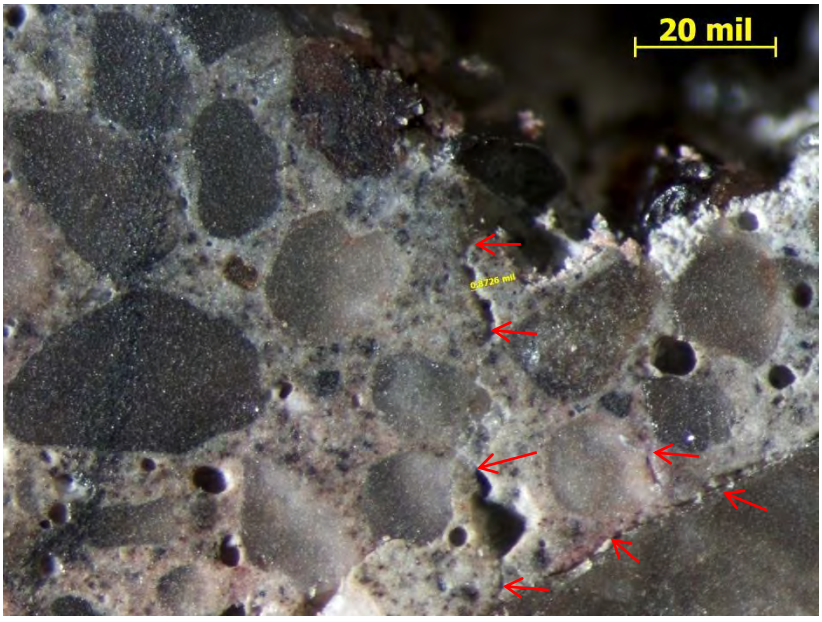

Figure 2. Lapped surface of Core 8 just below the top. The main microcrack split into a few tiny microcracks (indicated by red arrows) just below the very top surface of the core.

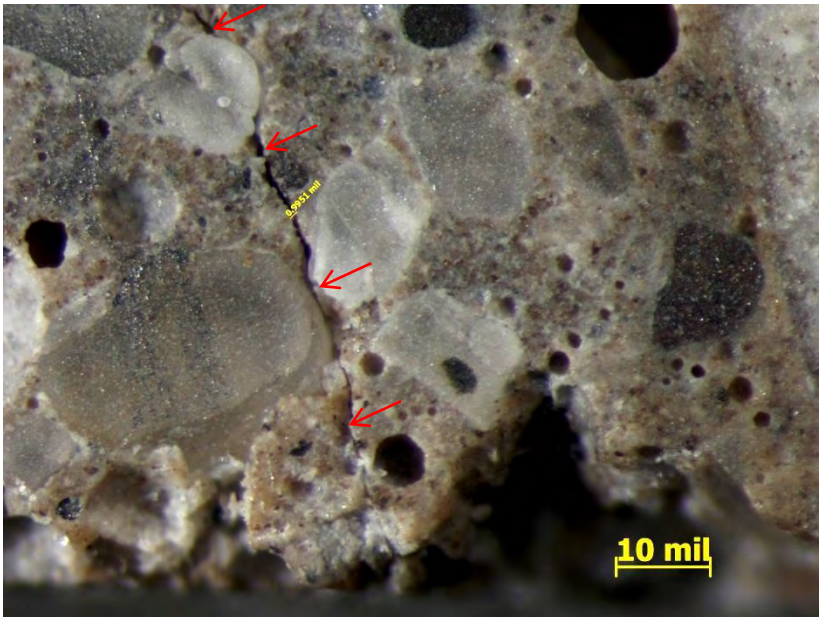

Figure 3. Shown is a microcrack (indicated by red arrows) on the lapped surface in bottom region of Core 8.

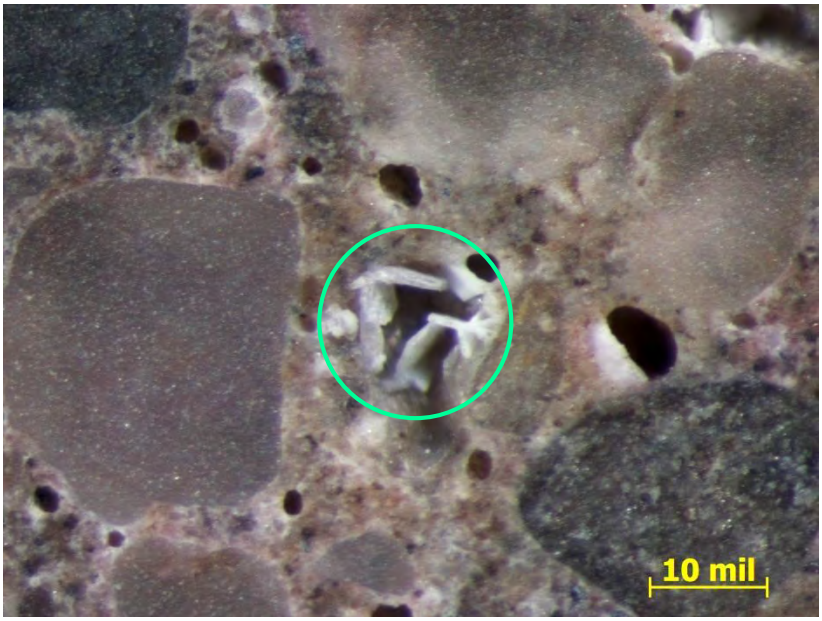

Figure 4. Lapped surface just below the top of Core 8 showing secondary deposits of calcium hydroxide inside an air void (encircled).

WJE ENGINEERS ARCHITECTS MATERIALS SCIENTISTS

APPENDIX D

Laboratory Analysis of Reinforcing Bars

LABORATORY EXAMINATION OF REINFORCING BAR SAMPLES

Galvanized reinforcing bars were removed from concrete cores taken from the topside of the bridge deck. Excess concrete was removed from the bars where possible. Selected bars were examined to evaluate the corrosion product, the degree of pitting, and the thickness of the zinc layer. The bar samples were selected to encompass a range of chloride levels within the concrete. Sample 8 had a very low level of chloride at the bar (0.004 percent by mass). Samples 3 and 7 had slightly higher levels of chloride at the level of the bar (0.050 and 0.084 percent by mass, respectively). Samples 9 and 10 had significantly higher levels of chloride at the level of the bar (0.193 and 0.376 percent by mass, respectively).

Evaluation of the Corrosion Product

The corrosion product on the exterior of the bar samples was evaluated visually using a stereomicroscope, and two specimens were further analyzed to determine composition.

Visual and Microscopical Evaluation

Sample 8 (low chloride level)
The bottom surface of Sample 8 has areas of both light green-gray shiny surface and dark gray surface. White deposits are present in limited areas. The top surface of the bar is uniform dark gray indicating the absence of corrosion. Light white discoloration may indicate minor surface corrosion of the bottom side of the bar. Photographs and micrographs of the sample are provided in Figure 1 through Figure 3.

Sample 3 (moderate chloride level)
The surface of Sample 3, where not covered with adherent concrete, was light gray, shiny with a metallic appearance on the bottom of the bar. White deposits were present in one area of the bottom of the bar indicative of zinc surface corrosion. The top of the bar had a darker gray appearance with the absence of notable corrosion. Photographs and micrographs of the sample are provided in Figure 4 through Figure 7.

Sample 7 (moderate chloride level)
The bottom surface of Sample 7 was lighter in color than the top surface. The appearance ranged from light gray to slightly green and shiny, to spots of white deposit, and a few spots of yellow-green deposit. Surface corrosion of the zinc is likely along the bottom surface of the bar. The top surface had more adherent concrete, but where the bar was exposed, was a uniform dark gray and corrosion was absent. Photographs and micrographs of the sample are provided in Figure 8 through Figure 12.

Sample 9 (high chloride level)
The bottom surface of Sample 9 is covered primarily in white corrosion deposits, although some localized areas have no apparent deposit. The top surface is primarily red corrosion product, with some white corrosion product present. This indicates that the zinc layer has been mostly consumed. Photographs and micrographs of the sample are provided in Figure 13 through Figure 15.

Sample 10 (high chloride level)
The bottom surface of Sample 10 consists primarily of white and red corrosion product, with some gray surface visible. The top surface consists primarily of red corrosion product, with a stripe of blue-gray deposit near the side of the bar. Corrosion is wide spread and the zinc has been consumed in areas. Photographs and micrographs of the sample are provided in Figure 16 through Figure 20.

Compositional Analysis of Corrosion Product

Compositional analysis of Sample 8 (low chloride) and Sample 10 (high chloride) was performed using scanning electron microscopy with energy dispersive x-ray spectroscopy (SEM/EDS). The corrosion products of Sample 10 were further analyzed using x-ray diffraction (XRD).

In SEM, a beam of electrons is generated, focused, and scanned across a very small area of the sample. The electrons interact with the sample in many ways, which can be used to image and analyze the sample. Two imaging modes are possible: backscattered and secondary. During backscattered electron (BE) imaging, the electron beam bombards the sample, and some electrons are backscattered or elastically scattered by the elements in the sample based on their atomic number. Heavier atoms in the sample scatter the beam electrons more than lighter atoms; hence phases with a higher average atomic weight appear brighter in the resulting image than phases with a lower average atomic weight, providing compositional information within the image. Secondary electron (SE) imaging uses electrons that are emitted from the sample as a result of inelastic interactions with the beam. SE images provide information related to the topography of the specimen; cracks and crystals deposited on the surface will be well defined. The interaction of beam electrons with the sample also generates characteristic x-rays. The energy of the characteristic x-rays can be measured using an EDS, and the elements present in the sample can be identified. EDS can only identify elements heavier than boron (carbon through uranium); therefore lighter elements, such as hydrogen, do not appear in the spectrum. EDS data can be collected from a point a few microns across, or over a larger area of the sample. Prior to analysis by SEM/EDS a sample is typically coated by a thin layer of conductive carbon. This carbon is apparent in the EDS spectrum. Therefore, for some samples, it cannot be determined if the carbon is from the sample itself or the carbon coating.

In addition to imaging and EDS spectra, the SEM can generate a dot map. In x-ray dot mapping mode the localized distributions of selected elements are shown in separate boxes. Each box is labeled to identify the element being represented in that box. The presence of an element in an area on the sample is indicated by a concentration of dots.

XRD analysis is suitable for identifying crystalline compounds; non-crystalline compounds do not have a definite XRD pattern. During x-ray diffraction analysis, radiation produced from an x-ray source is diffracted off the sample at various angles. A detector measures the intensity of the diffracted energy, and the location (angle) and intensity are recorded as a graph. This graph, which displays a pattern of peaks, can be interpreted to identify the crystalline components of the sample. The peaks are compared to a library of diffraction patterns of known components.

Sample 8 (low chloride level)

Sample 8 had a distinct dual-color appearance, with the top of the bar (as it was placed in the slab) having a dark gray appearance, with a lighter gray/silver/white appearance on the bottom of the bar (Figure 21). To evaluate compositional differences between the two colors, the surface of Sample 8 was examined using SEM/EDS.

No significant compositional differences were observed between the darker and lighter portions of the bar (Figure 22 and Figure 23). Both consist primarily of zinc and oxygen, with varying amounts of calcium, and small quantities of aluminum, silicon, sulfur, lead, chromium, and iron. The zinc is from the

galvanizing layer, the oxygen is present either as some oxidation of the zinc or from residual cement paste adhered to the bar. The calcium, aluminum, silicon, and sulfur are present from residual cement paste. The lead is present as an impurity in the zinc. The iron and chromium may be present from the bar itself.

Sample 10 (high chloride level)

A cross-section of Sample 10 was examined using SEM/EDS to evaluate the composition of the corrosion product and zinc layer. A large pit filled with iron corrosion product was examined. Significant, but varying, amounts of chlorine were detected in different layers of the corrosion product (Figure 24). This confirms a chloride-induced pitting mechanism. Examination of the zinc layer indicated corrosion (oxidation) beginning at the exterior (Figure 25). Little to no chlorine (beyond the small amount present in the epoxy mounting medium) is present in the zinc layer that is beginning to corrode.

A small amount of concrete remained adhered to the rebar of Sample 10 in the location prepared for cross-sectional analysis. This portion was examined in detail to determine if the corrosion product diffused into the concrete. Dot map analysis indicated that iron and zinc corrosion product penetrated through cracks in the concrete, but do not appear to have diffused into the concrete itself (Figure 26). It is not known if the cracks existed prior to the corrosion of the reinforcing bar.

White corrosion product (from corrosion of the zinc layer) was removed from Sample 10 for analysis using XRD. XRD detects crystalline components of a material. Unlike SEM/EDS, which provides elemental composition, XRD provides the ways in which the elements are combined. However, not all corrosion products are crystalline, so XRD does not provide a complete picture of all compositions present, and typically is used in conjunction with SEM/EDS. XRD analysis of white corrosion product from Sample 10 indicated the presence of zincite (ZnO) and zinc hydroxide [$Zn(OH)_2$], both common corrosion products of zinc.

Coating Thickness Measurements

Sections of bars from Cores 3, 7, 8, 9, and 10 were examined to determine the presence and thickness of zinc coating. The bars were cut in cross-section, embedded in a thermoset resin, and polished to produce a surface suitable for microscopy. To measure the thickness of the zinc layer, the cross-sections were examined using a reflected light microscope. Measurements were made using a calibrated scale reticle in the eyepiece. Twelve measurements were collected on Sample 8 and 4 (3/4 inch diameter, #6 bars), while twenty measurements each were collected on Samples 7, 9 and 10 (1-1/4 inch diameter, #10 bars). Results are presented in Table 1. Measurements of 0.0 mils indicate that no zinc layer was present at that location.

The thickness measurements indicated that metallic zinc is present in areas while completely corroded through in others. Samples 9 and 10 both exhibited surface corrosion, including white corrosion (zinc) and red corrosion (steel) and came from cores with significant chloride concentrations at the bar level. Pitting and significant zinc loss was also observed on Samples 9 and 10. The greatest degree of pitting was observed on the top surfaces (as placed in the slab) on both Samples 9 and 10. In contrast, little corrosion product was observed on Samples 3, 7, or 8. No difference in zinc layer thickness or degree of corrosion was apparent around the circumference of the bar; the thickness of zinc was the same on the top and bottom of the bar. Most of the zinc was consumed in Sample 9 and Sample 10 and pitting corrosion of the mild steel was noted. Micrographs showing the general condition of the zinc layers on the bar samples are provided in Figure 27 through Figure 35.

Table 1. Zinc Coating Thickness Measurements.

Reading	Zinc Coating Thickness (mils)				
	Sample 8	**Sample 3**	**Sample 7**	**Sample 9**	**Sample 10**
1	4.8	3.7	5.0	4.5	2.6
2	3.9	4.2	6.4	2.2	1.6
3	7.5	4.2	8.7	0.0	0.0
4	4.1	3.4	3.1	0.0	0.0
5	3.5	5.1	9.0	0.0	0.0
6	5.7	6.1	8.4	0.0	0.0
7	3.0	4.1	6.1	2.3	0.0
8	3.5	3.3	4.2	0.0	7.0
9	4.1	2.2	7.0	0.0	3.0
10	4.1	3.7	6.7	0.0	6.7
11	4.9	5.2	6.9	0.0	8.7
12	6.1	3.8	6.5	0.0	4.2
13			7.8	0.0	5.4
14			8.0	0.0	6.3
15			6.9	0.0	2.9
16			5.5	2.7	4.0
17			5.6	2.4	0.3
18			4.4	1.9	6.6
19			7.5	0.0	5.9
20			8.9	4.3	0.0
Minimum	3.0	2.2	3.1	0.0	0.0
Maximum	7.5	6.1	9.0	4.5	8.7
Average	4.6	4.1	6.6	1.0	3.3
Chloride content at bar level	0.004	0.050	0.084	0.193	0.376

Conclusions

The bars are hot-dipped galvanized and the zinc coating looks typical for this type of galvanizing. The zinc coating thickness in the samples exposed to 0.084 percent by mass of chloride were nominally similar and averaged between 4.1 and 6.6 mils, with individual measurements ranging from 2.2 to 9.0 mils. In this range of chloride concentrations, the zinc coating thickness of the bars did not appear to be affected by chloride, and it appears that these values are representative of the original coating thickness.

Samples 3, 7, and 8 were in chloride concentrations less than 0.084 percent and had intact zinc layers at every location measured around the circumference of the bar. They did contain limited white corrosion product present on the surface, most often on the underside of the bar. This underside corrosion may be due to incomplete contact with the concrete due to the minor settlement of the concrete away from the bottom of the bars or due to the trapping of bleed water beneath the bars. It is not uncommon for concrete settlement and bleed to alter the contact area of the bottom sides of reinforcing bars supported on chairs.

Significant loss of zinc thickness and underlying steel corrosion was observed in the two samples with chloride concentration greater than 0.193 percent by mass of chloride. Samples 9 and 10, from heavily chloride contaminated concrete, had intact zinc layers present only intermittently on the surface, and had pitting and red rust present on the surface. Sample 10, which had the highest chloride level, had the greatest amount of pitting present along the circumference studied.

The surface composition of Sample 8, chosen to represent a bar in non-chloride-contaminated concrete, consisted primarily of zinc, with some oxygen, and elements from the concrete that remained adhered to the surface. Although minimal oxidation of the surface was apparent from SEM/EDS analysis, the vast majority of the zinc layer was uncorroded.

Analysis of Sample 10, chosen to represent a corroded bar in chloride contaminated concrete, indicated the presence of chloride-induced corrosion in the pits, but little chlorine present in the intact or lightly corroding zinc layer.

Kimberly A. Steiner

Figures

Figure 1. Sample 8. Top side (left) and bottom side (right).

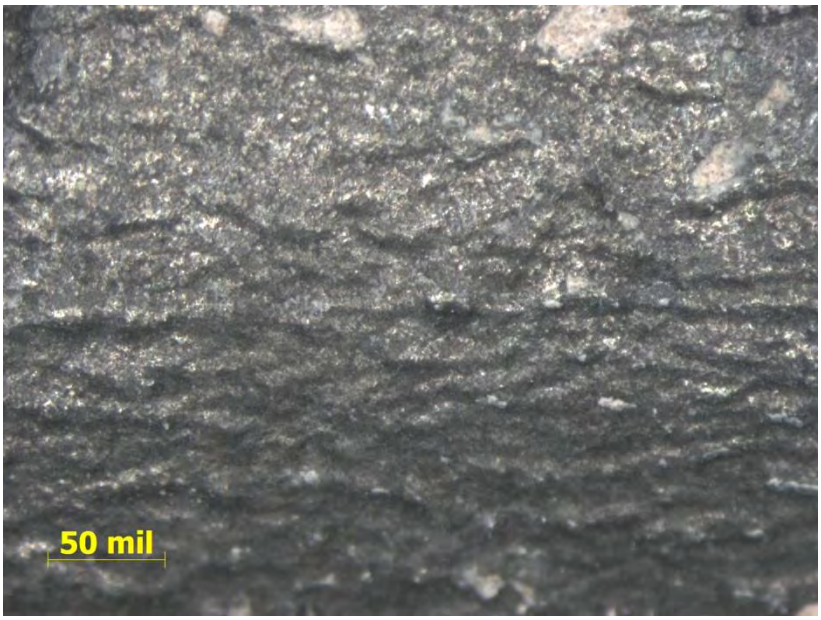

Figure 2. Micrograph of the top side of Sample 8. Note the uniform dark surface.

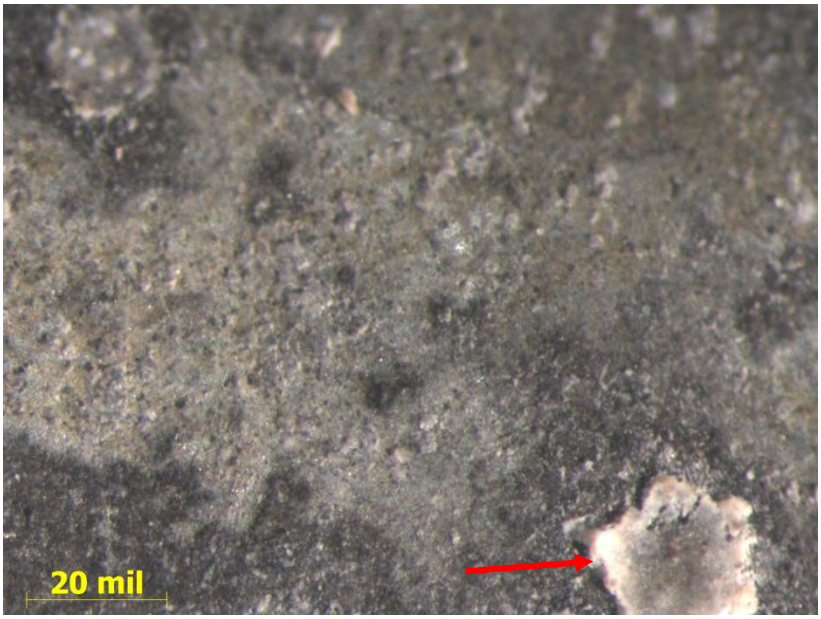

Figure 3. Micrograph of the bottom side of Sample 8. Note the dark to light coloration, with some white deposit indicated with an arrow.

Figure 4. Sample 3. Top side (left) and bottom side (right).

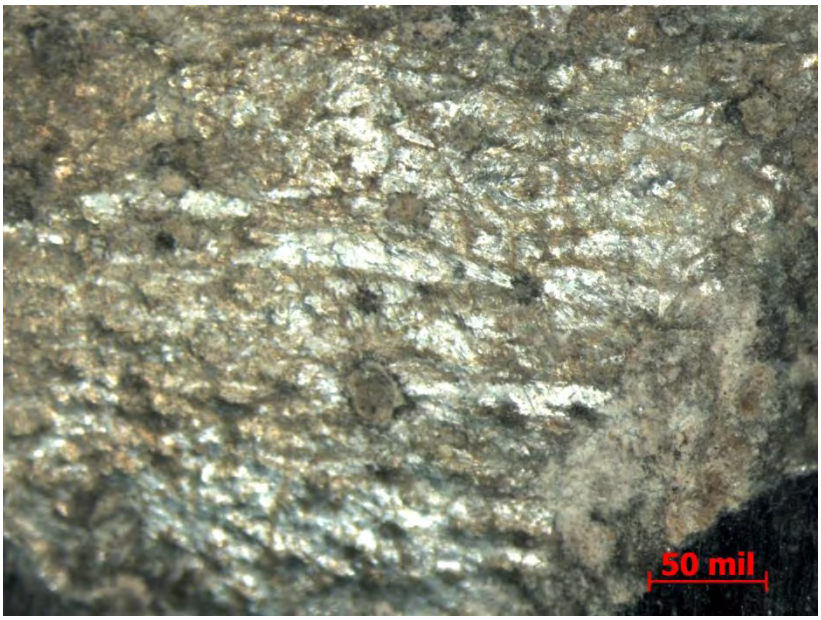

Figure 5. Micrograph of the bottom of Sample 3, showing the gray shiny surface.

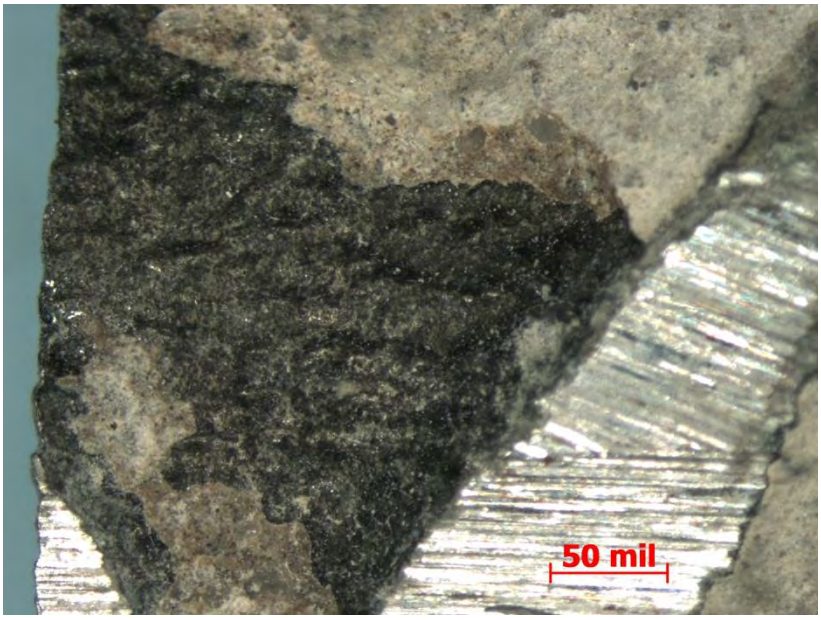

Figure 6. Micrograph of the top surface of Sample 3, showing the gray surface. The lighter color material on the surface is residual concrete.

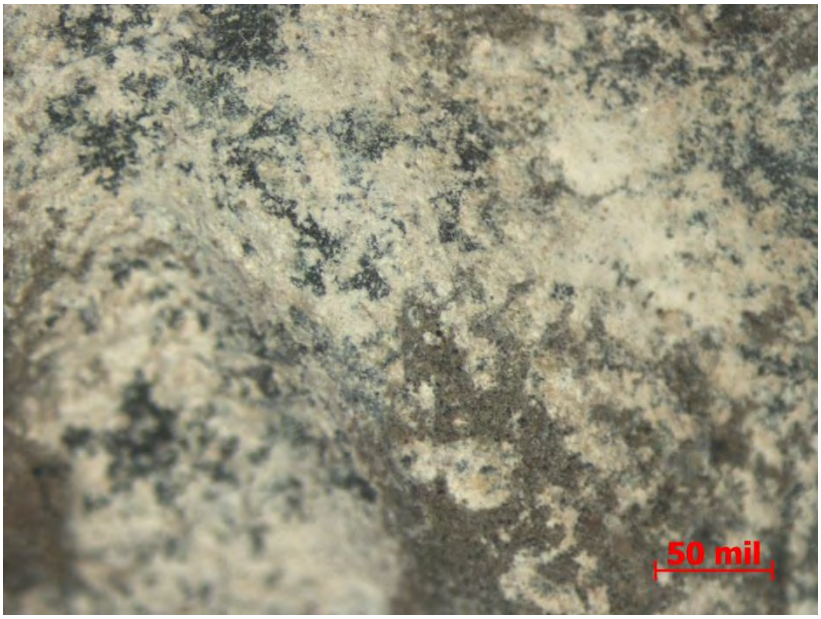

Figure 7. Micrograph of the top surface of Sample 3, showing white deposits.

Figure 8. Sample 7. Top side (left) and bottom side (right).

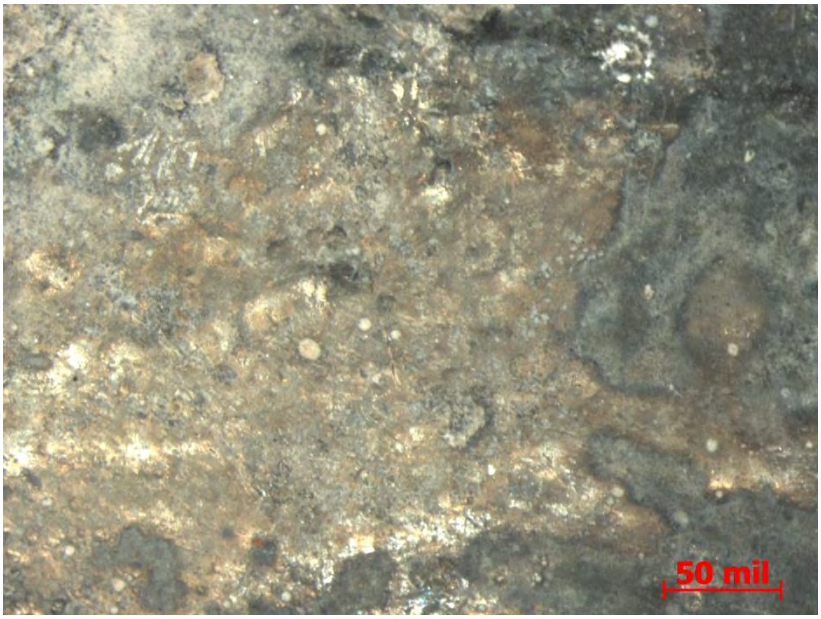

Figure 9. Micrograph showing the light green-gray shiny surface on the bottom of Sample 7.

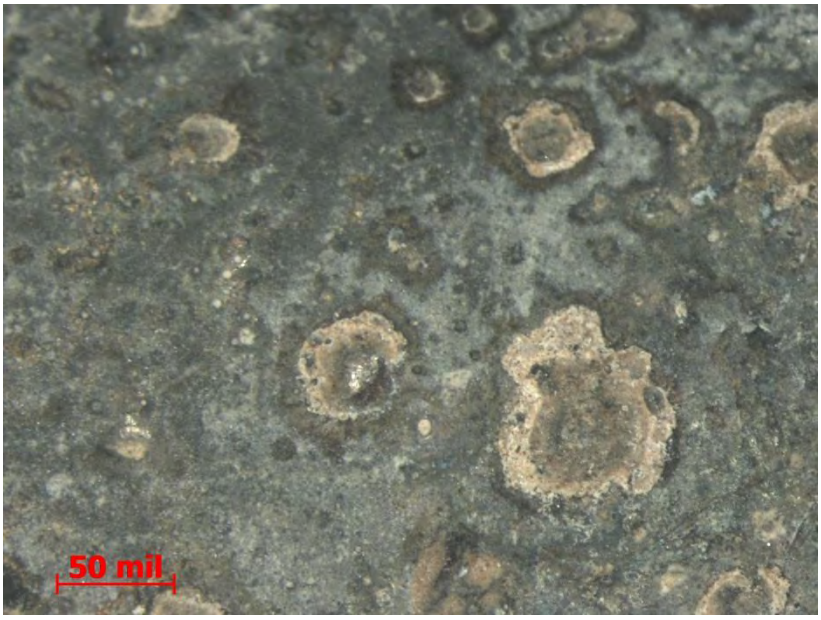

Figure 10. Micrograph showing the light gray surface of the bottom of Sample 7. The lighter colored deposits are adhered concrete.

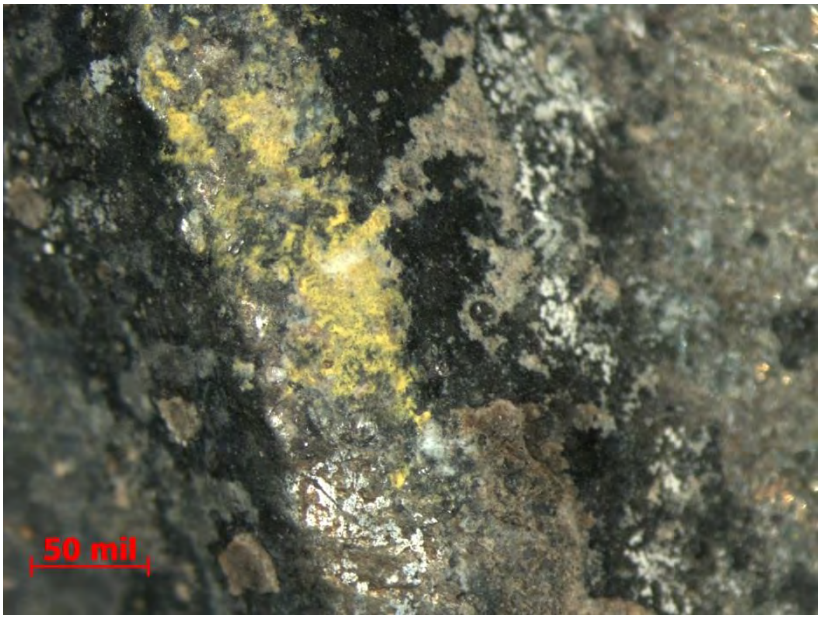

Figure 11. Micrograph sowing the yellow-green and white deposits on the bottom of Sample 7.

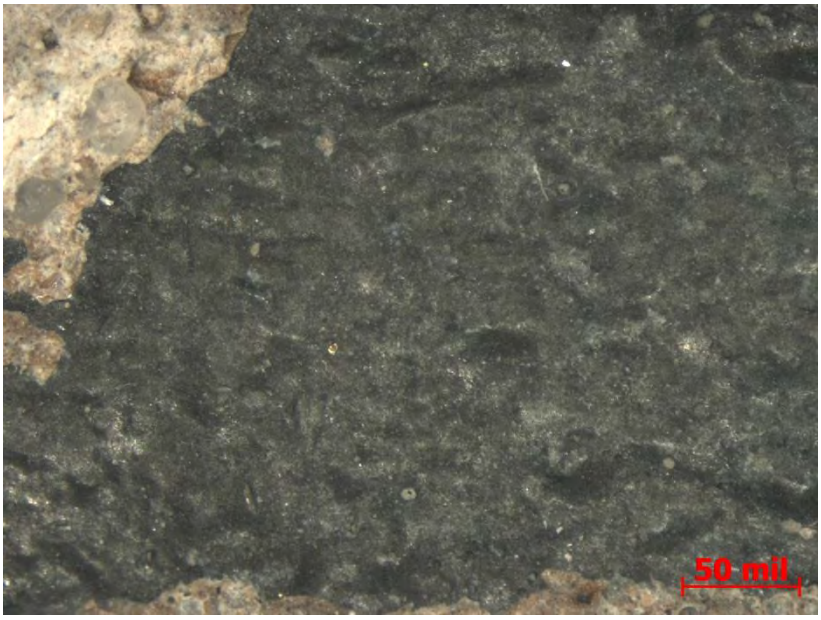

Figure 12. Micrograph showing the uniform, dark surface of Sample 7.

Figure 13. Sample 9. Top side (left) and bottom side (right).

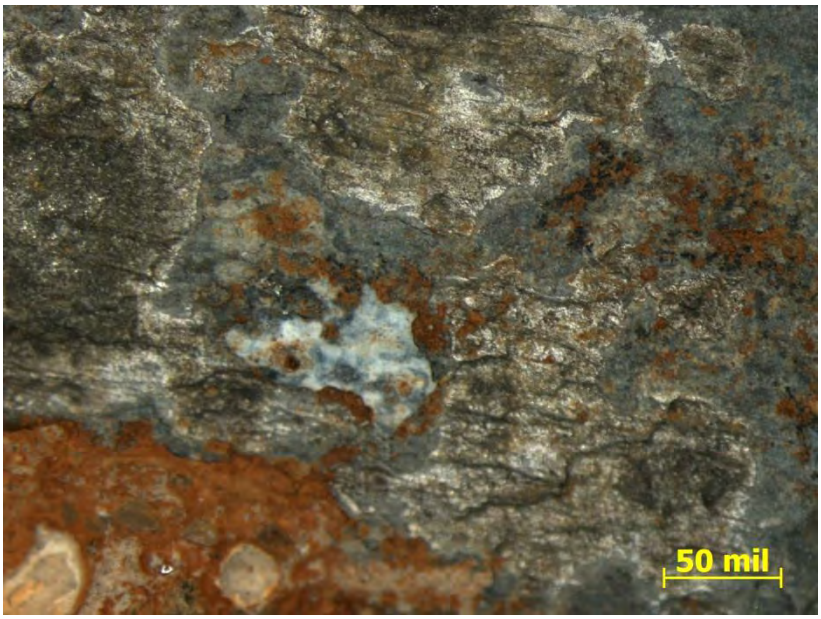

Figure 14. Micrograph of the bottom surface of Sample 9, showing localized areas with no deposits, nearby areas of white and red deposits.

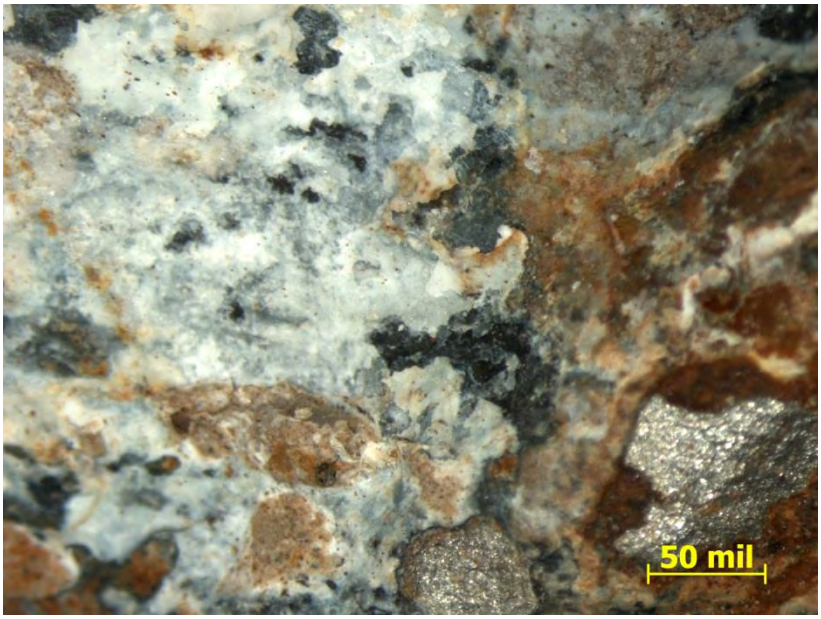

Figure 15. Micrograph of the bottom surface of Sample 9, showing white corrosion product.

Figure 16. Sample 10. Top side (left) and bottom side (right).The stripe of blue-gray deposit is indicated with an arrow.

Figure 17. Micrograph of the top surface of Sample 10, showing red corrosion product from the steel.

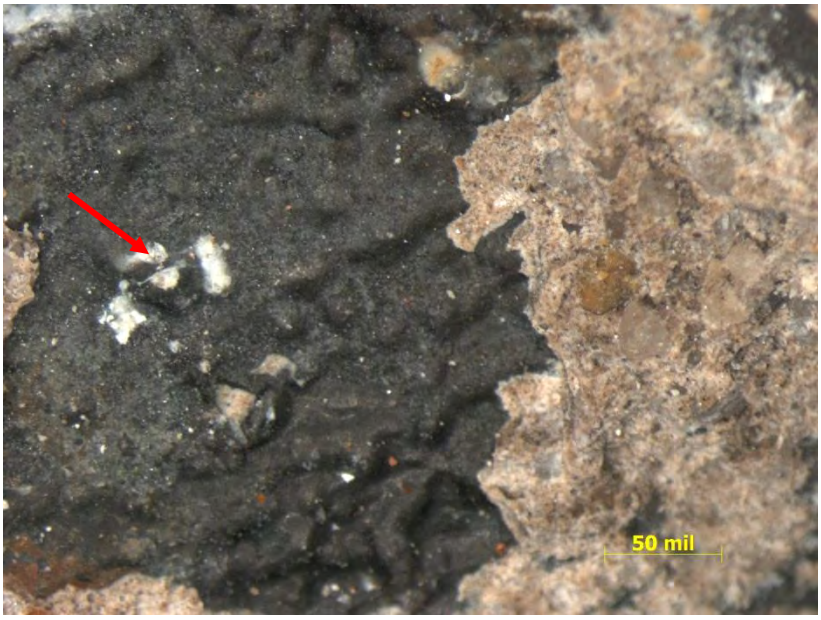

Figure 18. Micrograph of the side of Sample 10, showing concrete (indicated with an arrow) and a dark gray surface with only a small amount of white corrosion product.

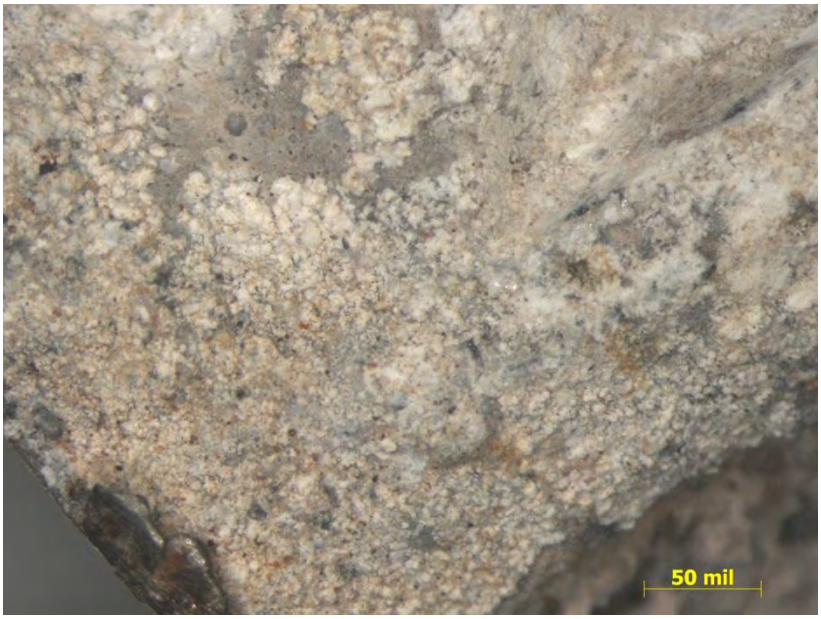

Figure 19. Micrograph of the bottom surface of Sample 10, showing a white deposit.

Figure 20. Micrograph of the blue-gray deposit on the side of Sample 10.

Figure 21. Photograph of Sample 8, showing the dual colors. An arrow indicates which side faced up in the slab.

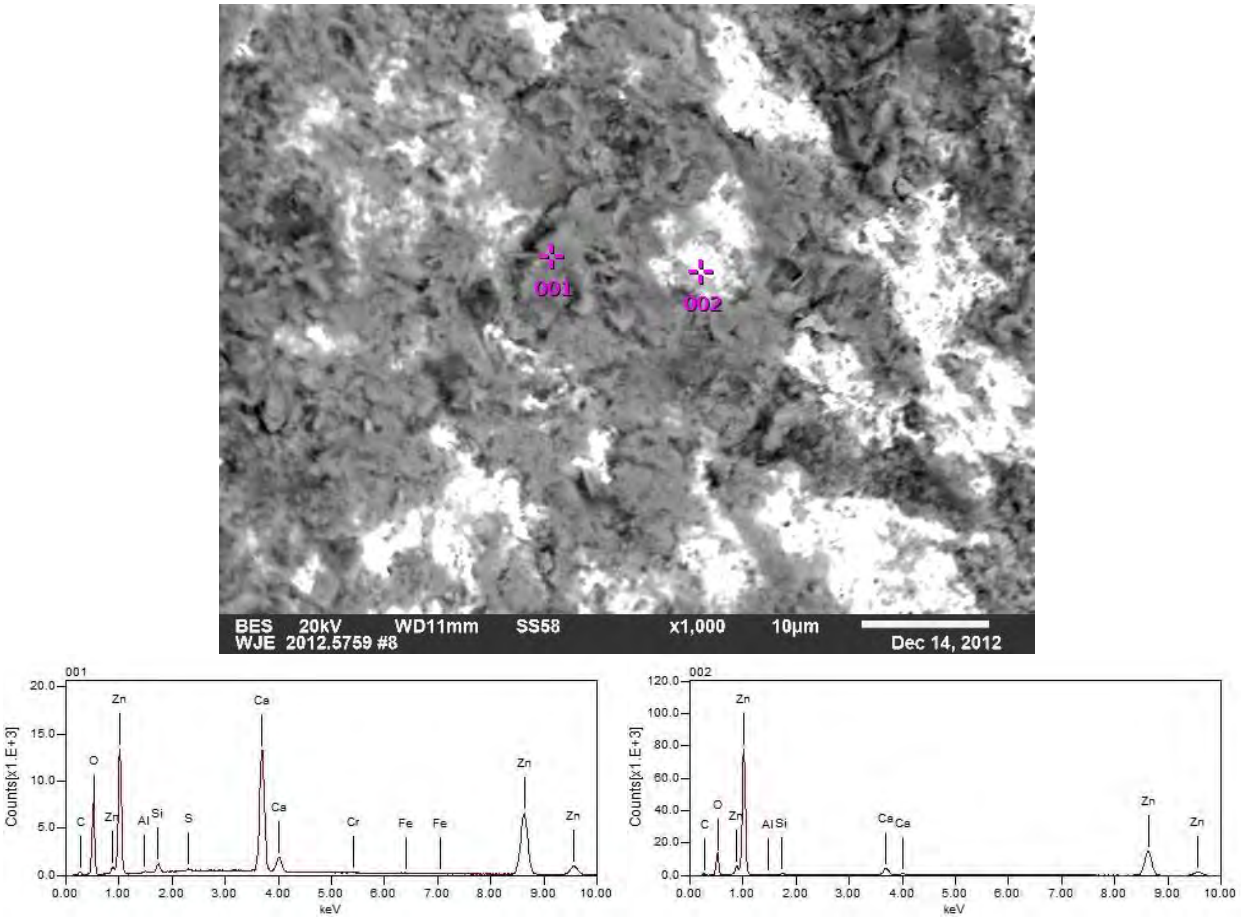

Figure 22. BE micrograph and point EDS spectra from the dark portion (top) of Sample 8. Each EDS spectrum has a number above the upper left corner which corresponds to the location indicated on the micrograph.

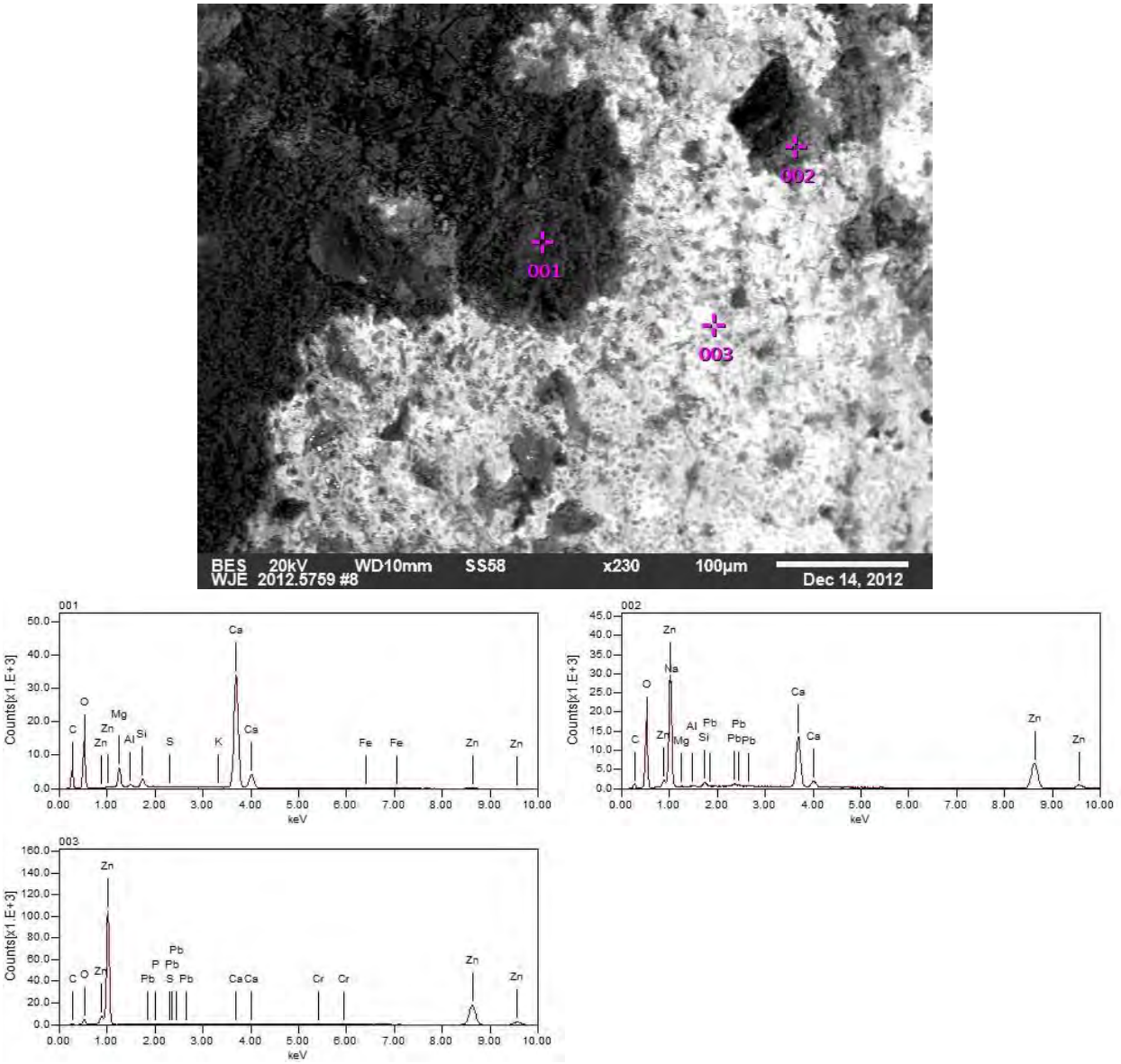

Figure 23. BE micrograph and point EDS spectra from the light portion (bottom) of Sample 8. Each EDS spectrum has a number above the upper left corner which corresponds to the location indicated on the micrograph.

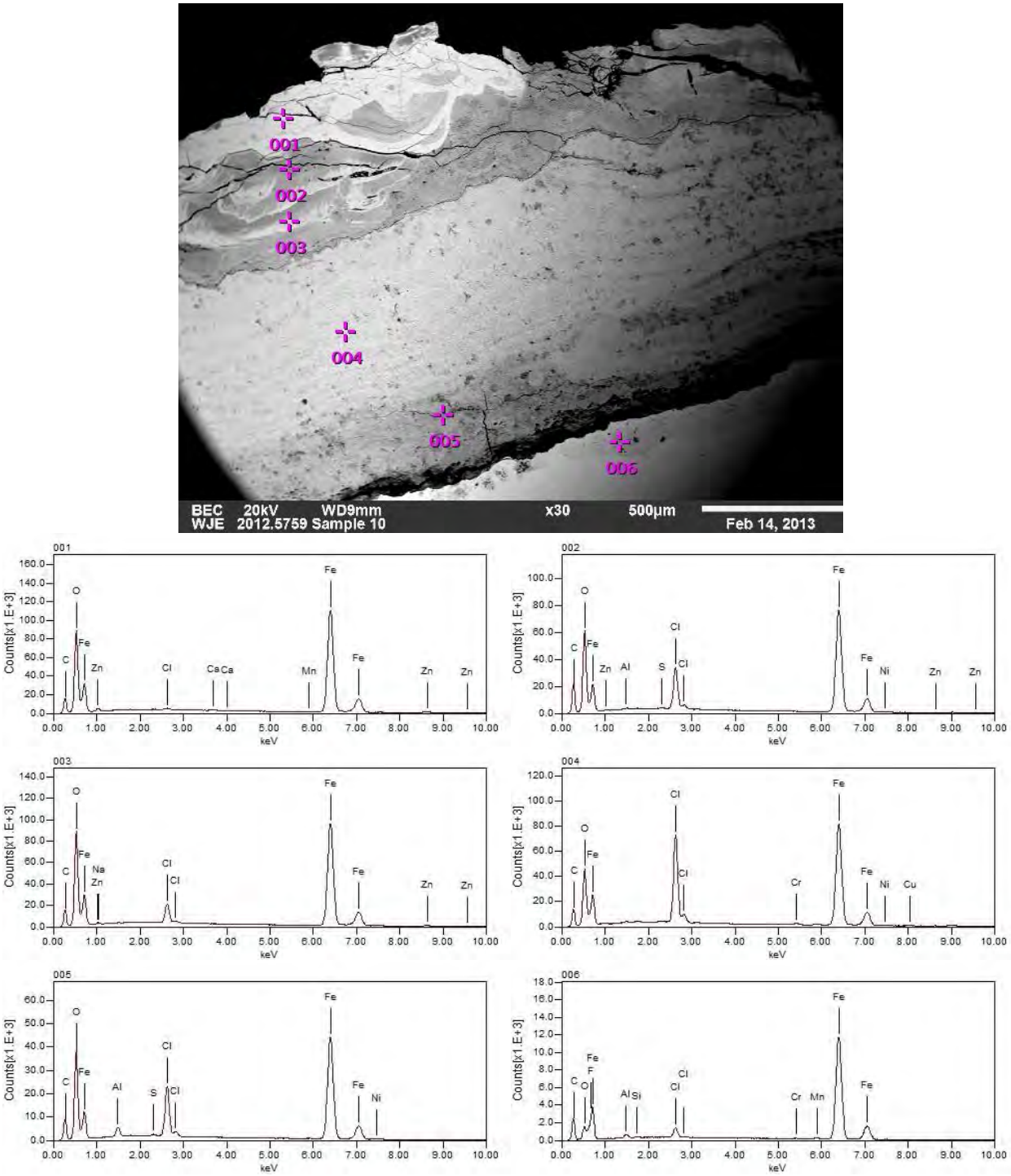

Figure 24. Cross-sectional BE image and point EDS spectra of a corroded pit on Sample 10, showing a significant amount of chlorine in the corrosion product. Each EDS spectrum has a number above the upper left corner which corresponds to the location indicated on the micrograph.

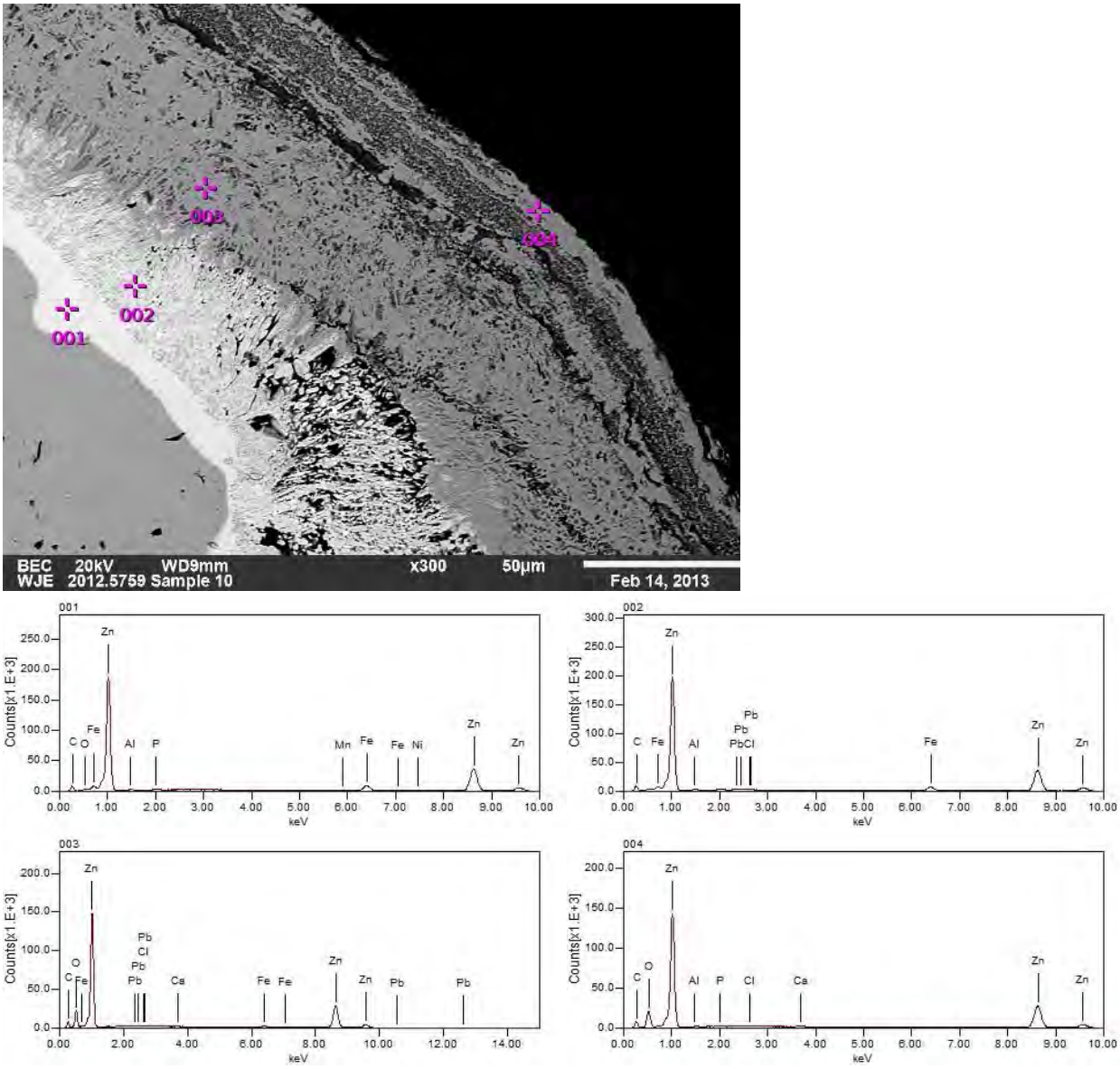

Figure 25. Cross-sectional BE image and point EDS spectra of the zinc layer Sample 10. Very little chlorine is incorporated into the zinc corrosion product (see EDS 004). Each EDS spectrum has a number above the upper left corner which corresponds to the location indicated on the micrograph. A minor amount of chlorine is present in the epoxy mounting medium.

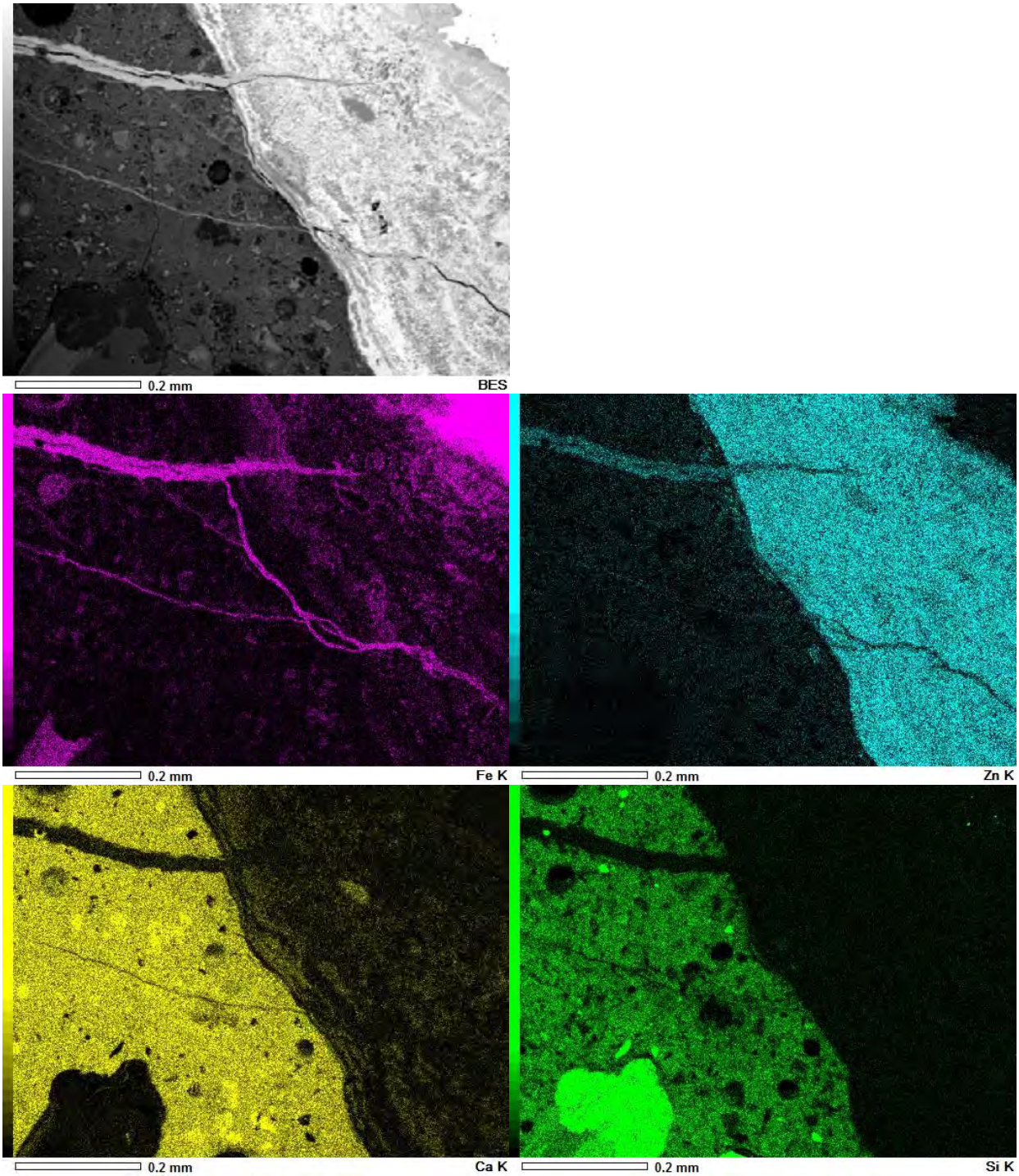

Figure 26. Dot map showing corrosion product/concrete interface of Sample 10. The corrosion product is on the right. The upper image is a BE micrograph. The elemental dot maps are, from left to right: purple -- iron, blue -- zinc, yellow -- calcium, green -- silicon. The iron and zinc can be seen penetrating the concrete along cracks, where calcium and silicon (constituents of cement paste) are not present.

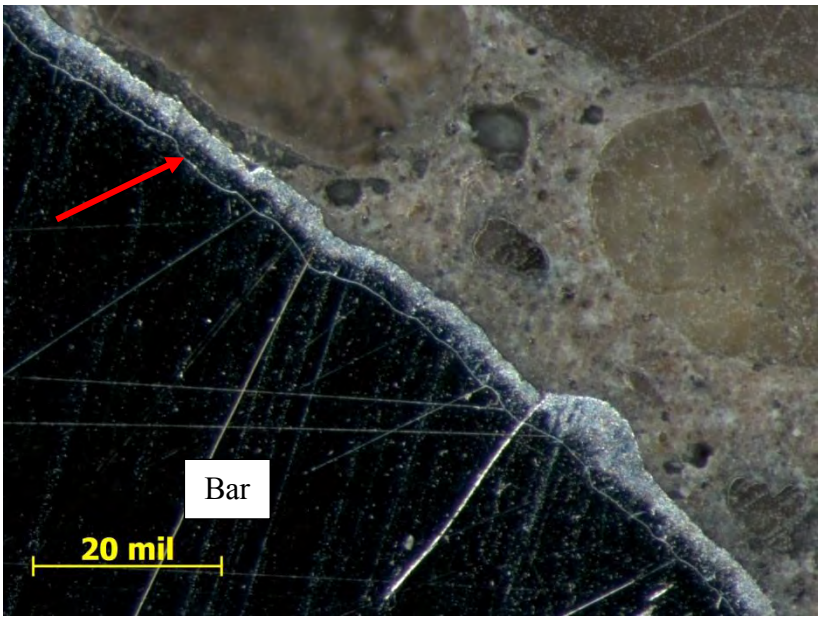

Figure 27. Cross-section of Sample 3, showing the bar, the zinc layer (arrow), and concrete adhered to the bar.

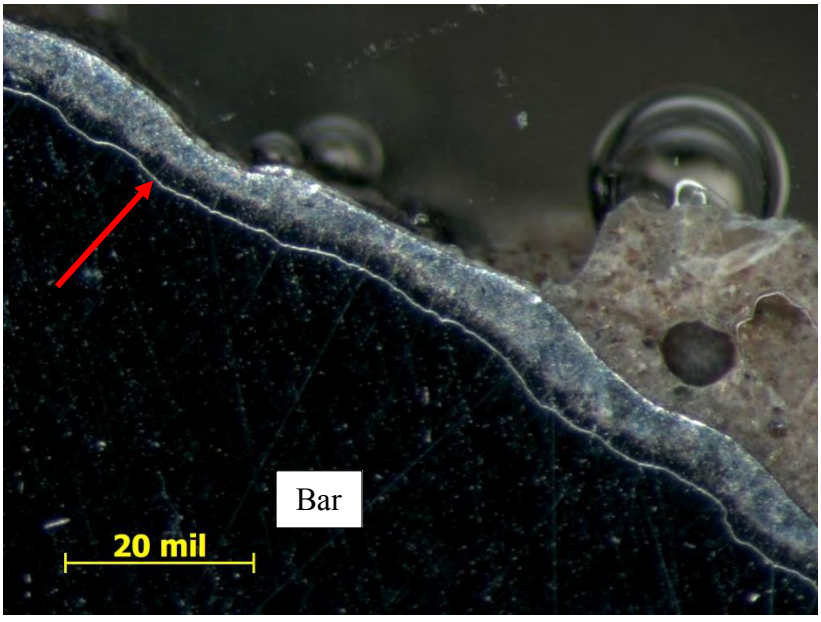

Figure 28. Cross-section of Sample 7, showing the bar (black), the zinc layer (arrow), and small section of concrete adhered to the bar. Epoxy (translucent bubbles), used in the preparation of the cross-section, is also present adhered to the zinc layer.

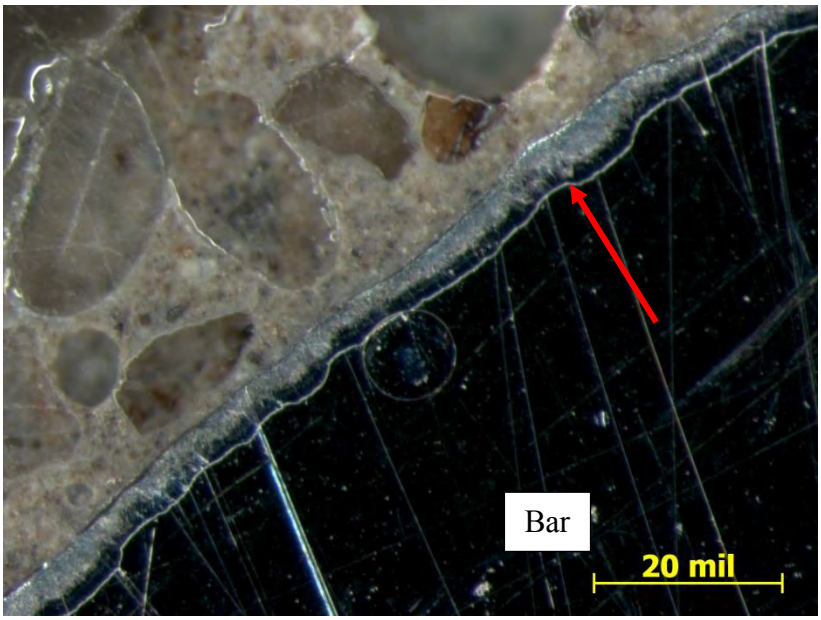

Figure 29. Cross-section of Sample 8, showing the bar (black) and the zinc layer (arrow), and concrete adhered to the bar.

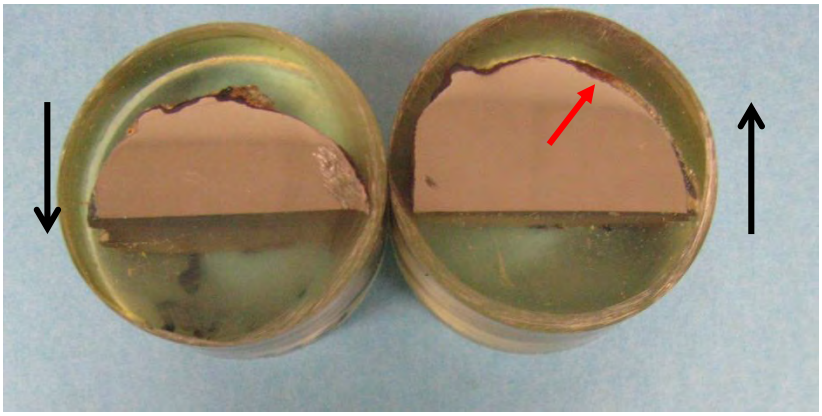

Figure 30. The polished cross-sections of Sample 9. The bar was cut in half so it could be placed into the epoxy molds. Arrows indicate which side was facing up in the slab. Some pitting can be seen on the top surface of the right-hand specimen (red arrow).

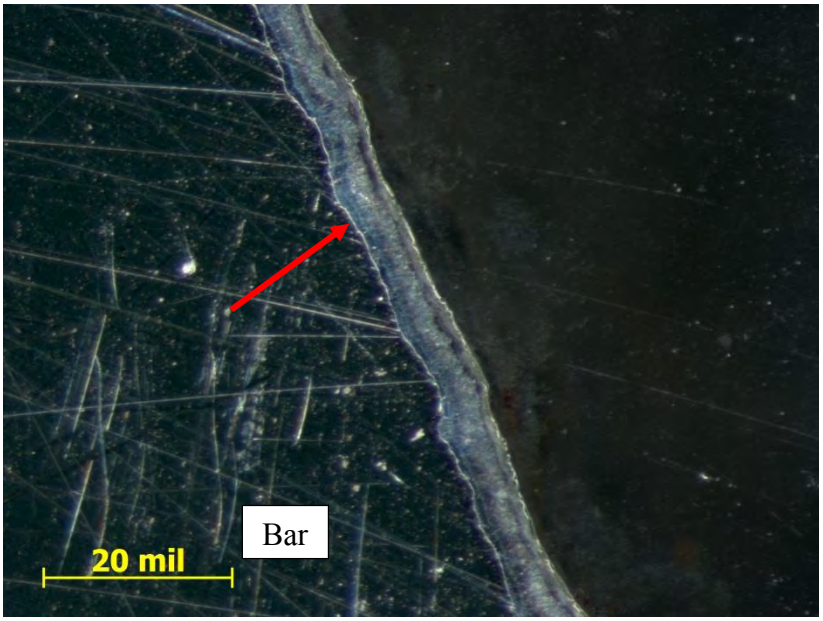

Figure 31. Cross-section of Sample 9, showing the bar and an intact zinc layer (arrow).

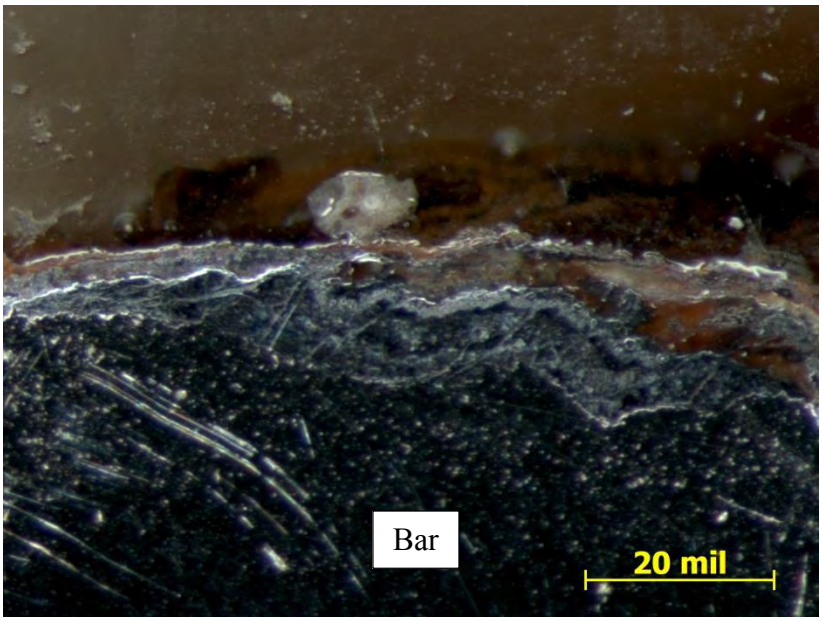

Figure 32. Cross-section of Sample 9, showing corroded bar.

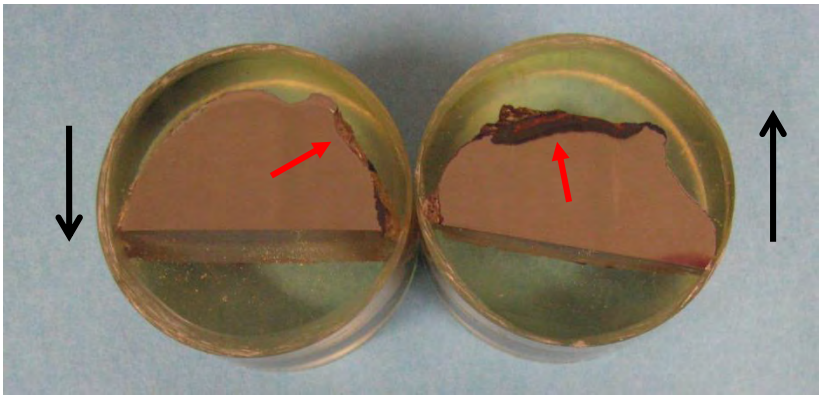

Figure 33. The polished cross-sections of Sample 10. The bar was cut in half so it could be placed into the epoxy molds. Arrows indicate which side was facing up in the slab. Significant pitting can be seen on the top surface of the right-hand specimen, and minor pitting can be seen on the bottom surface (red arrows).

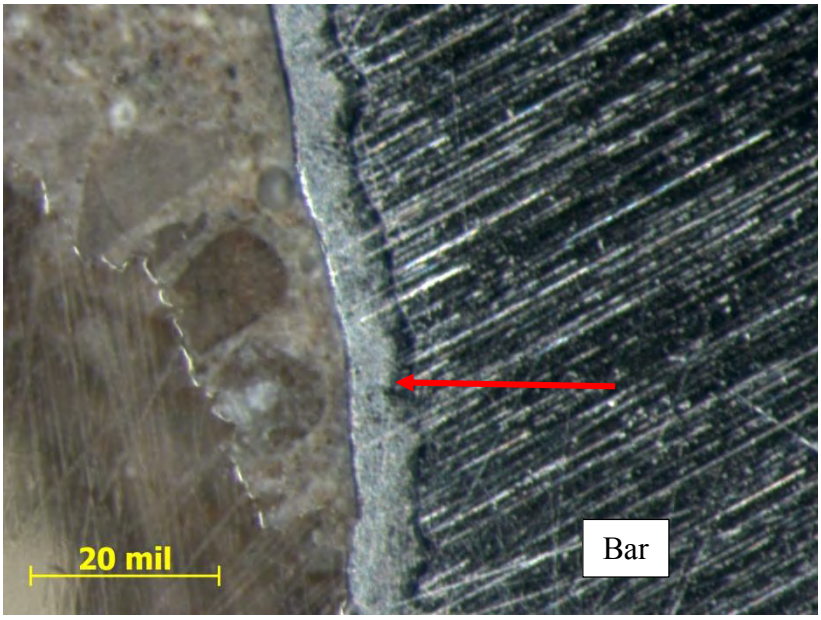

Figure 34. Cross-section of Sample 10, showing the bar, the intact zinc layer (arrow), and concrete adhered to the bar.

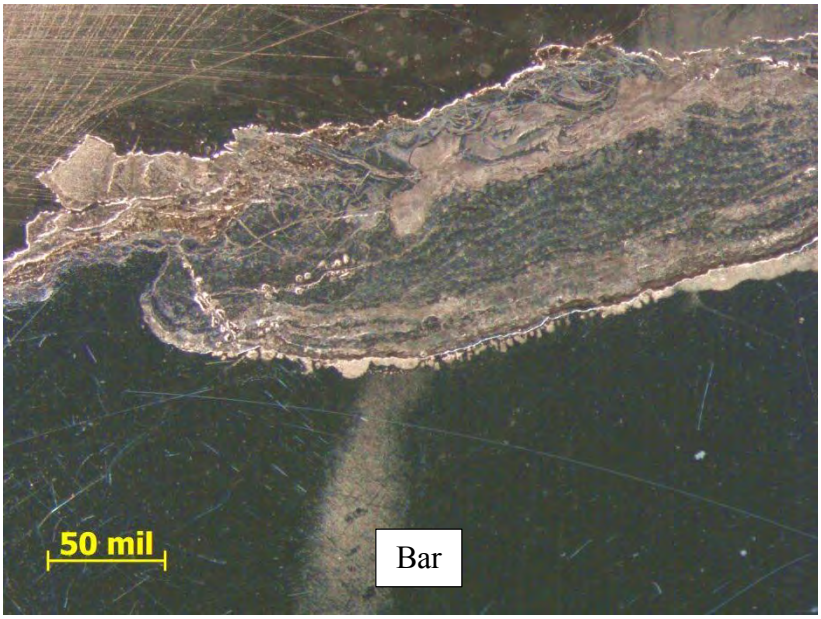

Figure 35. Cross-section of Sample 10, showing the corroded bar and pitting corrosion.

WJE ENGINEERS ARCHITECTS MATERIALS SCIENTISTS

APPENDIX E

Follow-Up Site Visits

WJE ENGINEERS ARCHITECTS MATERIALS SCIENTISTS

Wiss, Janney, Elstner Associates, Inc.
330 Pfingsten Road
Northbrook, Illinois 60062
847.272.7400 tel | 847.291.5189 fax
www.wje.com

APPENDIX E - FOLLOW-UP SITE VISITS

Introduction

As a follow-up to the evaluation of the performance of galvanized reinforcing bars in the bridge deck of Iowa State Highway 92 over Drainage Ditch #25 in western Louisa County, Iowa, John Lawler of Wiss, Janney, Elstner Associates, Inc. (WJE) visited the project site during deck repair operations, which were performed subsequent to our evaluation of this bridge deck. The deck repair work included milling the top surface of the bridge deck, the removal and replacement of concrete at areas of delamination, casting a concrete overlay over the entire bridge deck, and installing new joints. To keep the bridge open to traffic, the repairs to the bridge deck were performed on one-half of the bridge at a time, with the contractor beginning work in the Fall of 2013 on the westbound lanes, and with the eastbound lanes being repaired during the Spring of 2014. As a result, WJE made site visits on October 7, 2013 and April 2, 2014, in both cases after concrete repair work had begun. The objectives of the site visits were to observe repair operations, to inspect the conditions of the bars exposed by the repair process, and to verify that any conditions of distress observed after deck surface milling were consistent with observations of the deck top surface made during the WJE field investigation.

At the time of these visits, the top 1/4-in. of the deck surface had been milled off, the deck had been sounded to identify delaminations, and the delaminations had been removed by chipping, leaving the tops of reinforcing steel exposed. In addition, the concrete surrounding the top mat of reinforcing at the joints had been removed in a strip approximately 2 feet wide. Figures E1 to E4 show representative views of the deck and repair openings in the westbound lanes, while representative views of the deck and repair openings in the eastbound lanes are provided in Figures E5 through E8. Subsequent repair procedures not witnessed by WJE were to include: sandblasting or shotblasting the concrete surface, installation of new joints, and placement of a concrete overlay.

Review of Proposed Coating Repair Materials

Prior to the start of the deck repair work, WJE consulted with the contractor to help them select a material to repair locations of damaged coating on the reinforcing bars exposed at the deck repair openings. IaDOT specifications indicate that a coating should be applied to any bare reinforcing steel exposed during repair of bridge decks with epoxy-coated reinforcing bars, but similar guidance is not provided for galvanized reinforcing. In theory, the galvanizing layer on a reinforcing bar can be restored by using a zinc-based coating, but an epoxy-based product for coating reinforcing bars could also be effective because it would electrically isolate the reinforcing bar in the repair openings. After several communications regarding this topic, it is our understanding that the contractor elected to use a zinc-rich anti-corrosion coating designed for use on reinforcing steel.

Methods

During both site visits, WJE inspected the repair openings, performed a delamination survey by chain drag of the deck surface, and measured the thickness of the galvanizing layer on exposed bars by electromagnetic thickness gauge (Elcometer 456 Coating Thickness Gauge).

Findings and Discussion

Repairs

Most repair openings were generally localized and were directly associated with corrosion of a single reinforcing bar. In a number of cases where two reinforcing bars were exposed during excavation, only one appeared to be actively corroding (see Figure E6). The corrosion was generally associated with cracks that were in-line with the corroded bar (see Figure E9).

The repair excavations at corroding reinforcing bars generally extended only to the top surface of the exposed reinforcing bars, as can be seen in Figures E2, E3, E6, E7, and E8. This location defined the bottom of the delamination and the extent of the "unsound" concrete, so all delaminated concrete was being removed. We understand that the applicable IaDOT specifications give the bridge engineer the responsibility for establishing the depth of repair, stating the following: "Removal for Class A repair extends at least to the level of the top reinforcing bars, and deeper, as determined by the Engineer, to remove unsound concrete." In addition, we understand that the general policy is that if more than half of the bar diameter is exposed, the entire bar should be exposed. Therefore, the amount of concrete removal we observed was consistent with IaDOT specifications and project requirements. Additionally, the extent of concrete removal was generally consistent with the extent of delaminated concrete identified by WJE during the 2012 field investigation.

While the observed repair openings at locations of reinforcing corrosion generally did not expose more than half the bar, we generally recommend that repair of concrete damage due to chloride-driven corrosion should include removal of concrete around the entire perimeter of the bar to at least 3/4 in. below the corroded bar section. This practice is discussed extensively in the literature, including in ICRI 310.1R-2008 *Guideline for Surface Preparation for the Repair of Deteriorated Concrete Resulting from Reinforcing Steel Corrosion*. While removal of concrete below the bars may include removing otherwise sound concrete, the intent is to remove concrete with elevated levels of chloride so as to re-establish passive conditions at the bar by encapsulating the bars in new, uncontaminated repair concrete. This will reduce the risk of corrosion initiating on the bar below the interface with the repair material and increase the life of the repair. Note that this does not address the potential for the ring-anode (or "halo") effect, a process by which corrosion in bars adjacent to concrete repairs is accelerated by locally large differences in the internal concrete environment at the perimeter of patch repairs. However, coating the reinforcing bars exposed in a repair opening with an electrically insulating coating such as an epoxy would reduce the risk of ring-anode corrosion by increasing the resistance path within the repair.

Concrete removal not directly related to corrosion damage had been performed at the ends of the decks and the west approach slab on the eastbound lane apparently to allow for the installation of a new joint seal system. The concrete removal at these repair openings was performed to a depth below the top layer of reinforcing steel, as can be seen in Figure E4. The epoxy coating on the reinforcing exposed in the approach slab was damaged as shown in Figure E10. The contractor indicated that a coating patch material would be applied to the bars prior to concrete installation, as required by IaDOT specifications. Even with this repair, it should be recognized that the protection afforded to the reinforcing steel by the original fusion-bonded epoxy coating has been reduced.

Finally, partial depth concrete removal had also been performed around the deck scuppers (Figure E11), reportedly to accommodate elevation modifications associated with the new overlay. The cover at the drains will be less, somewhat reducing the corrosion protection at this already vulnerable site.

Galvanizing thickness

The results of the galvanizing layer thickness testing are given Table E1. As expected, the thickness of the galvanizing layer varied depending on the level of corrosion of the reinforcing bars. If significant corrosion had occurred, such as shown in Figure E12, less zinc was present and thickness measurements from 0 to 3.9 mils were recorded. However, where no corrosion product was visible, the galvanizing thickness ranged from 5.2 to 8.0 mils. These values are consistent with the thicknesses measured during the 2013 work.

Modeling

A primary component of WJE's 2012 investigation was quantifying the corrosion resistance of the galvanized reinforcing in terms of a corrosion threshold and propagation time, as implemented in a service life model, based on the observed rate of distress development calculated from information available from surveys or repair projects of the bridge deck conducted in 2006 and 2009, and the 2012 WJE survey. To assess the progression of damage between WJE's 2012 deck survey and the recent repairs, WJE identified new deterioration by comparing the repair areas with the results of the 2012 delamination survey of the deck. A combined total of 4.1 sq. ft. of additional delamination was observed during the October 2013 and Spring 2014 site visits, bringing the total estimate of distress up to 131.6 sq. ft., which corresponds to 4.2 percent of the total deck area. While additional damage was observed, the interval between measurements was only one year, so the fact that the increase in damage was small is not surprising.

In Figure E13, this percentage of damage is added to the prior observations of damage and the damage projected through service life modeling that was shown in Figure E13. This new data point falls well within the range of damage projected based on the range of assumed chloride thresholds and propagation times. Therefore, a modification to WJE's quantification of corrosion resistance (ranging from a chloride threshold of 0.095 percent by weight with a propagation time of 18 years to a chloride threshold of 0.188 percent by weight with a propagation time of 5 years) is not warranted based on this information.

Tables

Table E1. Thickness of zinc coating on bars exposed in repair areas

Location	Westbound		Eastbound	
	Thickness (mils)	Steel corrosion product visible?	Thickness (mils)	Steel corrosion product visible?
1	5.9	No	5.8	No
2	5.9	No	6.2	No
3	5.7	No	7.8	No
4	8.0	No	5.2	No
5	5.3	No	3.7	Yes
6	3.9	Yes	2.0	Yes
7	0	Yes	7.3	No
8	7.9	No		
9	7.9	No		

Figures

Figure E1. Overall view of IA92 deck, westbound lanes during Oct. 7, 2013 site visit.

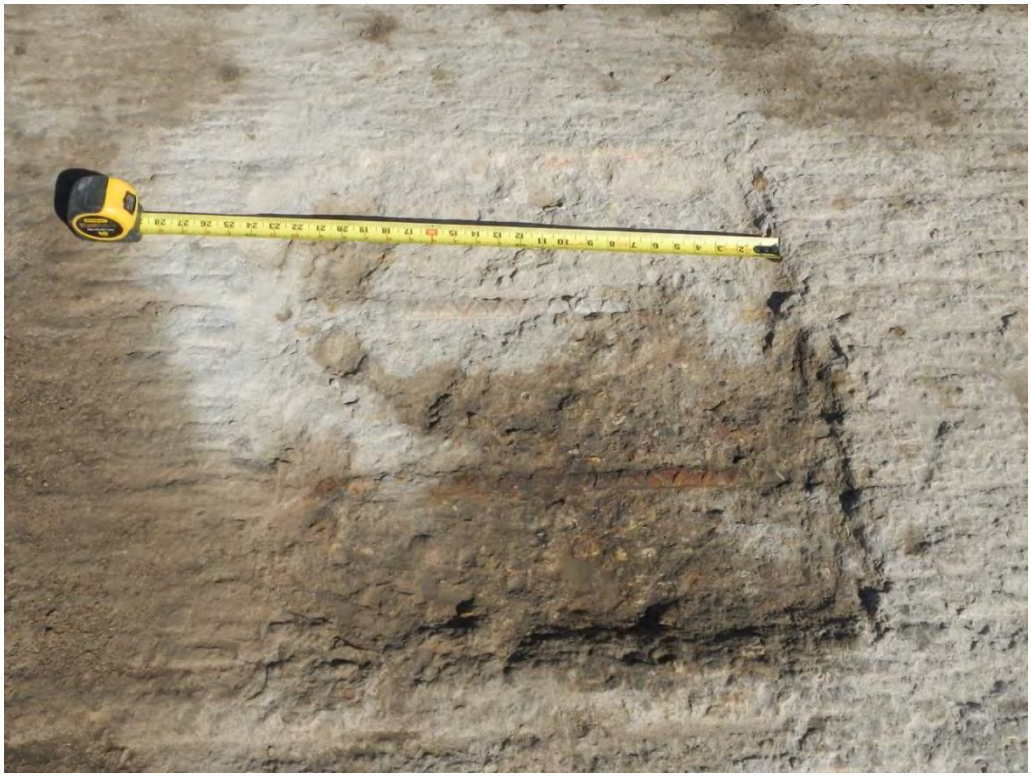

Figure E2. Close-up of typical repair location in IA92 deck, westbound lanes.

Figure E3. Typical repair location in IA 92 deck, westbound lanes

Figure E4. Deeper removal along end joint at westbound lanes

Figure E5. Overall view of IA92 deck, eastbound lanes during April 2, 2014 site visit.

Figure E6. Close-up of repair location in IA92 deck, eastbound lanes.

Figure E7. Typical repair location in IA 92 deck, eastbound lanes.

Figure E8. Deck repair location extending from deeper repair at end joint in eastbound lanes of IA 92 deck.

Figure E9. Corroding bar at crack (yellow line) in eastbound lanes.

Figure E10. Damage to epoxy coating on bars in west approach slab in eastbound lanes

Figure E11. Concrete removal at scupper drain on westbound lane.

Figure E12. Close-up of corroded bar in westbound lanes.

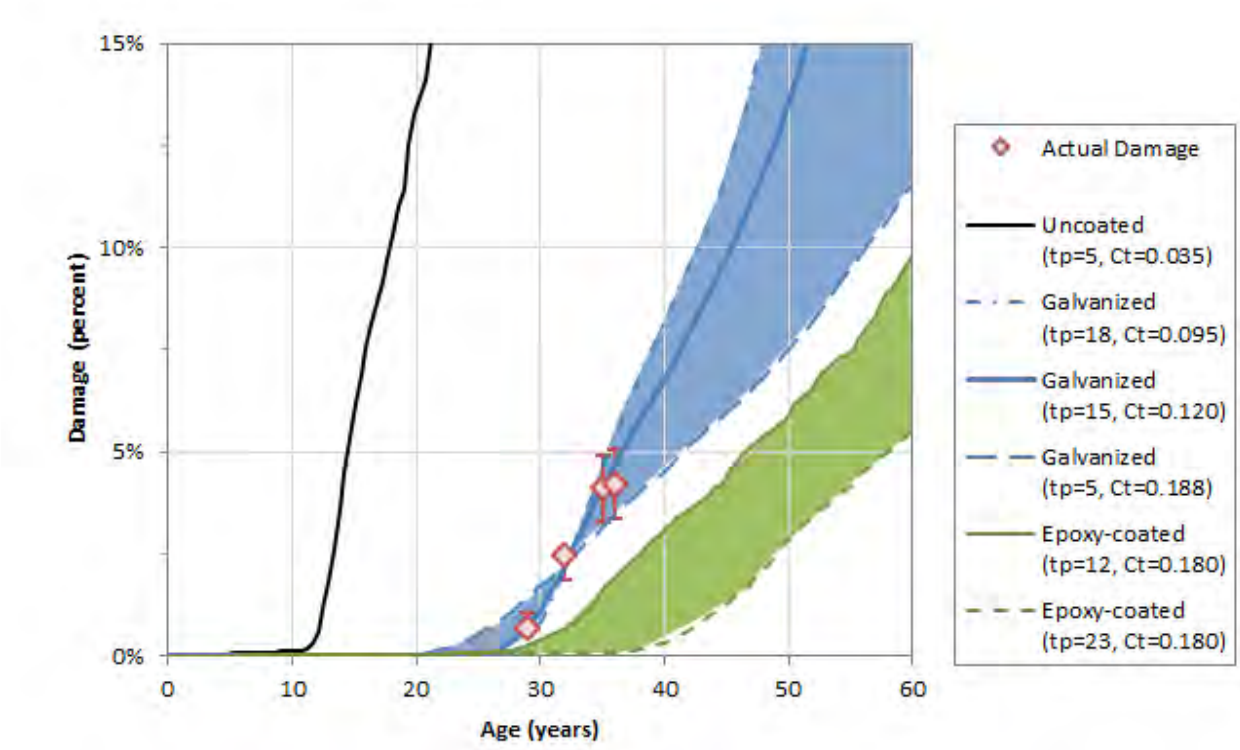

Figure E13. Results of service life model for bridge - updated to show additional distress through 2013/2014. (Propagation time (tp) is given in years, and chloride threshold (Ct) is given in percent by weight of concrete.)